# Were early Archean carbonate factories major carbon sinks on the juvenile Earth?

Wanli, Xiang[1, 2], Jan-Peter, Duda[2], Andreas, Pack[3], Mark, van Zuilen[4], Joachim, Reitner[2, 5]

[1] College of Tourism and Geographical Science, Leshan Normal University, Leshan, 614000, China.

[2] Department of Geobiology, University of Göttingen, Göttingen, 37077, Germany.

[3] Department of Geochemistry and Isotope Geology, University of Göttingen, Göttingen, 37077, Germany.

[4] Naturalis Biodiversity Center, Leiden, 2333CR, The Netherlands.

[5] Göttingen Academy of Science and Humanities in Lower Saxony, Göttingen, 37073, Germany.

*Correspondence to*: Reitner Joachim (jreitne@gwdg.de)

**Abstract.** Paleoarchean carbonates in the Pilbara Craton (Western Australia) are important archives for life and environment on early Earth. Amongst others, carbonates occur in interstitial spaces of ca. 3.5–3.4 Ga pillow basalts (North Star-, Mount Ada-, Apex-, and Euro Basalt, Dresser Formation) and associated with bedded deposits (Dresser- and Strelley Pool Formation, Euro Basalt). This study aims to understand the formation and geobiological significance of those early Archean carbonates by investigating their temporal-spatial distribution, petrography, mineralogy, and geochemistry (e.g., trace elemental compositions, $\delta^{13}C$, $\delta^{18}O$). Three carbonate factories are recognized: (i) an oceanic crust factory, (ii) an organo-carbonate factory, and (iii) a microbial carbonate factory. The oceanic crust factory is characterized by carbonates formed in void spaces of basalt pillows (referred to as "interstitial carbonates" in this work). These carbonates precipitated inorganically on and within the basaltic oceanic crust from $CO_2$-enriched seawater and seawater-derived alkaline hydrothermal fluids. The organo-carbonate factory is characterized by carbonate precipitates that are spatially associated with organic matter. The close association with organic matter suggests that the carbonates formed via organo-mineralization, that is, linked to organic macromolecules (either biotic or abiotic) which provided nucleation sites for carbonate crystal growth. Organo-carbonate associations occur in a wide variety of hydrothermally influenced settings, ranging from shallow marine environments to terrestrial hydrothermal ponds. The microbial carbonate factory includes carbonate precipitates formed through mineralization of extracellular polymeric substances (EPS) associated with microbial mats and biofilms. It is commonly linked to shallow subaquatic environments, where (anoxygenic) photoautotrophs might have been involved in carbonate formation. In case of all three carbonates factories, hydrothermal fluids seem to play a key-role in the formation and preservation of mineral precipitates. For instance, alkaline earth metals and organic materials delivered by fluids may promote carbonate precipitation, whilst soluble silica in the fluids drives early chert formation, delicately preserving authigenic carbonate precipitates and associated features. Regardless of the formation pathway, Paleoarchean carbonates might have been major carbon sinks on the

early Earth, as additionally suggested by carbon isotope mass balances indicating a carbon flux of 0.76-6.5 $\times$ 10$^{12}$ mol/year. Accordingly, these carbonates may have played an important role in modulating the carbon cycle and, hence, climate variability, on the early Earth.

## 1 Introduction

Biogeochemical carbon cycling plays a crucial role in maintaining the stability of modern Earth's climate system (Ciais et al., 2013). It encompasses carbon fluxes between sources (e.g., volcanic and metamorphic $CO_2$) and various sinks (e.g., terrestrial silicate weathering, seafloor carbonatization, biomass build-up, deposition of carbonates and organic matter, carbon subduction into the mantle) (Ciais et al., 2013; Suarez et al., 2019). In case of carbon sinks, carbonates and organic matter stand out as the two paramount reservoirs (Gislason and Oelkers, 2014; Hoefs, 2018; Shields, 2019; Canfield, 2021). Out of these two reservoirs, carbonate rocks are particularly significant, serving as a primary carbon sink over geological timescales (Veizer et al., 1982; Nakamura and Kato, 2004; Canfield, 2021). Understanding the formation and evolution of carbonate factories—that is, conceptual models encompassing carbonate production and associated processes at various scales, from local precipitation to global sedimentation (Schlager, 2000; Schrag et al., 2013; Reijmer, 2021)—is therefore essential for comprehending the dynamics of the carbon cycle and its implications for climate change.

Throughout most of Earth's history, carbonate precipitation has been closely linked to biological processes, ranging from direct to indirect precipitation (that is, biologically controlled vs induced) (Flügel, 2010). Over the past couple of years, awareness has risen that carbonate precipitation can also be induced by organic matter (i.e., "organo-mineralization"), regardless of its origin (Addadi and Weiner, 1985; Reitner, 1993; Reitner et al., 1995a, b, 2000, 2001; Trichet and Défarge, 1995; Pei et al., 2021, 2022). Based on previous works about "cold-water carbonates" (Lees and Buller, 1972) and "mud-mound carbonates" (Reitner and Neuweiler, 1995), Schlager (2000) summarized three modern carbonate factories in the marine benthic zone, namely tropical shallow-water system, cool and deep-water system, and mud-mound/microbial buildup system. Since then, the carbonate factory concept has been extended across spatial and temporal scales (Pomar and Hallock, 2008; Reijmer, 2021; Pei et al, 2021, 2022; Wang et al., 2023). Despite these years of intense research, carbonate factories are still poorly understood, particularly during the Archean eon (4.0 to 2.5 billion years ago, Ga), when life on Earth was just in its infancy. During this eon, which accounts for about one-third of our planet's history, the Earth system experienced significant geobiological developments, such as declining volcanic activity and decreasing surface temperatures (Lunine and Lunine, 1998; Nisbet and Sleep, 2001; Lowe and Tice, 2007; Sengupta et al., 2020; Lowe et al., 2020; Reinhardt et al., 2024). Hence, geological and biological key-processes – and by extension Archean carbonate factories – must have been very different as compared to any later stage in Earth's history.

One of the most important early Earth records is the ca. 4.0–3.6 Ga Isua Supracrustal Belt (ISB; West Greenland), albeit being highly metamorphic (amphibolite facies: Nutman et al., 2019a, b). Rocks of the 3.5–3.2 Ga East Pilbara Terrane (EPT; Pilbara Craton, Western Australia) and the 3.6–3.2 Ga Barberton Greenstone Belt (BGB; South Africa) in contrast are well preserved in terms of metamorphism (prehnite-pumpellyite to greenschist facies, i.e. max. 250–300 °C: Van Kranendonk et al., 2019a; Hickman-Lewis et al., 2019) and hence provide valuable windows into early Archean carbon sinks. Indeed, rocks of the EPT are for instance well known to contain carbonates associated with microbial facies (i.e. stromatolites; Van Kranendonk, 2006, 2007; Allwood et al., 2006, 2007; Wacey, 2010; Lepot et al., 2013; Sugitani et al., 2015a) and pillowed basalts (Kitajima et al., 2001; Nakamura and Kato, 2002, 2004; Terabayashi et al., 2003; Marien et al., 2023) as well as carbonaceous organic matter (primarily preserved in chert and carbonate: Marshall et al., 2007; Bontognali et al, 2012; Duda et al., 2016, 2018; Flannery et al., 2018; Weimann et al., 2024; Mißbach et al., 2021). With regard to carbonates, most studies have focused on occurrences associated with microbial facies in the ~3.4 Ga Strelley Pool Formation, yet those constitute a minor component within the EPT lithostratigraphy (Van Kranendonk et al., 2007b).

Basaltic rocks of the EPT show evidence of pervasive carbonatization and silicification associated with hydrothermal processes in subaquatic environments (Kitajima et al., 2001; Nakamura and Kato, 2002, 2004; Terabayashi et al., 2003). Carbon flux estimates based on observations in this region suggest that hydrothermal carbonatization of pillowed seafloor basalts constituted a significant $CO_2$ sink in the early Archean (Nakamura and Kato, 2004). However, these estimates did not consider interstitial carbonates — that is, carbonates that precipitated in void spaces between pillow basaltic rocks (Marien et al. 2023; this work). Over the past few decades, the significance of carbon sequestration through hydrothermal alteration of oceanic crust has become obvious, underscoring the meaning of these processes for the global carbon cycle and, by extension, long-range climate regulation (Alt and Teagle, 1999; Bach et al., 2011; Coogan and Gillis, 2013; Krissansen-Totton et al., 2015, 2018). Indeed, more recent mass balance models for total organic carbon burial ($f_{org}$) take also authigenic carbonates, including those formed through oceanic crust carbonatization, into account (e.g., Krissansen-Totton et al. 2015). Nevertheless, the informative value of these approaches is limited due to the scarcity of theoretical frameworks and geological baseline data that would allow to constrain such additional carbon sinks, thereby impeding a comprehensive understanding of carbon cycle dynamics over geological time scales.

To address this issue, this study investigates early Archean carbonates in the EPT, including interstitial carbonates associated with basalts, carbonate stromatolites and other sedimentary carbonates. The combination of detailed petrography with mineralogical and geochemical analyses (e.g., trace elemental compositions, $\delta^{13}C$, $\delta^{18}O$) provides novel insights into the formation of carbonates during the early Archean. Based on this information, the fraction of carbon in the ocean being sequestered as inorganic and organic carbon was calculated and discussed with respect to overall carbon flux dynamics. The results of this study demonstrate the presence of various types of carbonate factories on the juvenile Earth and indicate that they might play a significant role in the early global carbon cycle and, hence, climate system.

## 2 Geological settings

95 The EPT (3.53–3.17 Ga) in Western Australia is famous for its well-preserved Paleoarchean volcano-sedimentary successions, which provide the world's most complete record of the evolution of the geo-, hydro-, bio- and atmosphere on the early Earth (Van Kranendonk et al., 2007a, b; Hickman and Van Kranendonk, 2012a, b). A particular interest is the Pilbara Supergroup, a 20 km thick succession of mainly volcanic rocks that can be subdivided into (from bottom to top) the Warrawoona Group (3.53–3.43 Ga), the Kelly Group (3.42–3.32 Ga), the Sulphur Springs Group (3.27–3.23 Ga), and the Soanesville Group (ca.

100 3.19 Ga) (Van Kranendonk et al., 2002, 2007b; Rasmussen et al., 2007; Hickman and Van Kranendonk, 2012a, b). The lower three groups comprise ultramafic to felsic volcanic rocks, chemical and clastic deposits, as well as swarms of subseafloor hydrothermal silica ± barite veins (Van Kranendonk, 2006). The tectonic setting of the EPT is controversial, ranging from mid-ocean ridge and island arc (Ueno et al., 2001; Komiya et al., 2002; Kato and Nakamura, 2003) to a thick ocean volcanic plateau (Smithies et al., 2003, 2005, 2007a, b; Van Kranendonk, 2006; Van Kranendonk et al., 2007a, b, 2019a).

105 A characteristic feature of the EPT is the so-called dome-and-keel structure, consisting of a central nucleus of the 3459 ± 18 Ma North Pole Monzogranite ("North Pole Dome") surrounded by little-deformed, predominantly mafic volcanic rocks of the Warrawoona Group and Kelly Group (Hickman and Van Kranendonk, 2012a) (Fig. 1). The oldest basaltic formation in this area is the North Star Basalt (3490 ±15 Ma Ar/Ar), which is overlain by the Dresser Formation (3481 ± 2 Ma U-Pb) consisting of chert ± barite beds and veins that are associated with pillowed basalts and dolerite (Van Kranendonk et al., 2008; Hickman

110 and Van Kranendonk, 2012b). Atop the Dresser Formation follows (from base to top) a ~ 4 km thick succession of mafic volcanic rocks (Mount Ada Basalt), a < 1.3 km thick succession of felsic volcanic rocks (Duffer Formation, Panorama Formation), and a < 150 m thick package of jasper (Marble Bar Chert Member, Towers Formation) (Byerly et al., 2002; Hickman and Van Kranendonk, 2012b). In the eastern part of the dome, the Panorama Formation is underlain by the Apex basalt (Nakamura and Kato, 2004), which is dated to 3463–3454 Ma based on zircon U-Pb ages of the underlying Duffer

115 Formation and the overlying Panorama Formation (Thorpe et al., 1992; McNaughton et al., 1993). Surrounding the central dome, the Panorama Formation is disconformably overlain by the Strelley Pool Formation (SPF, 3414 ± 34 Ma, U–Pb ages, Gardiner et al., 2019), which is known for its distinctive stromatolites (e.g., Lowe, 1980, 1983; Hofmann et al., 1999; Van Kranendonk et al., 2003; Allwood et al., 2006a; Hickman et al., 2011; Duda et al., 2016), followed by the high-Mg and tholeiitic Euro Basalt (3350 ± 3 – 3335 ± 7 Ma, GSWA, 2013) (Van Kranendonk et al., 2006; Hickman and Van Kranendonk, 2012b).
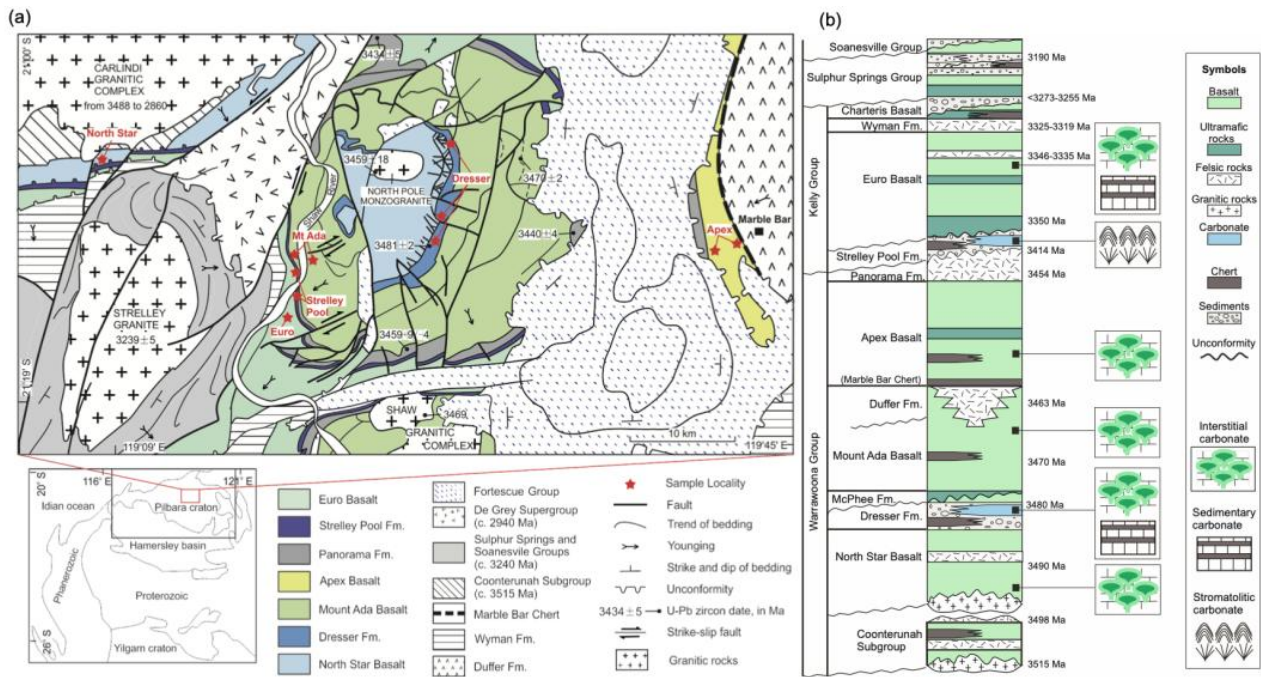
**Figure 1: (a) Simplified geological map of the North Pole Dome, Eastern Pilbara Terrane, Western Australia (adapted from Van Kranendonk and Hickman, 2000, Hickman and Van Kranendonk, 2012b) including sampling localities (red stars). (b) Simplified stratigraphy of the studied Archean rocks (adapted from Van Kranendonk et al., 2007b).**

## 3 Materials and methods

### 3.1 Sample locality

Paleoarchean carbonate rocks analyzed in this study derive from the North Pole Dome in the EPT (Fig. 1) and were collected from existing drill cores stored at the Geological Survey of Western Australia (Agouron Institute Drilling Project, AIDP) as well as during field campaigns organized by the German Research Foundation (DFG) Priority Program 1883 "Building a Habitable Earth" together with Australian colleagues. Interstitial carbonates were sampled from the ~3.49 Ga North Star Basalt (drill core 102 AIDP-1; 21°06'38"S, 119°06'4"E, French et al., 2015), the ~3.46 Ga Apex Basalt ("Schopf Locality" at Chinaman Creek; Schopf, 1993), the ~3.47 Ga Mount Ada Basalt and the ~3.35 Ga Euro Basalt (both near "Trendall Locality" at Shaw River; Hickmann et al., 2011), as well as from the Middle Basalt Member of ~3.48 Ga Dresser Formation (Dresser Barite Mine). Bedded sedimentary carbonates were sampled from the Dresser Formation at the "Tsunami Locality" (Runge et al. 2022) near the Dresser Barite Mine, and the Euro Basalt at the east side of the Shaw River near the "Trendall Locality". Stromatolitic carbonates were collected from the Strelley Pool Formation at the western side of Shaw River.

In order to better understand depositional environments of the studied EPT carbonates, we additionally analyzed the carbon and oxygen isotopic compositions of diverse reference materials for comparison. They include carbonate inclusions in black

barites from the Dresser Formation (drill cores PDP 2b and 2c), rhodochrosites in cherts from the ~3.25 Ga Fig Tree Group (Heinrichs, 1980; Rincon-Thomas et al 2016), carbonates of debated origin in the vicinity of the controversial ~3.7 Ga stromatolite site in the ISB in Greenland (Nutman et al., 2016; Allwood et al., 2018; provided by van Zuilen, 2018), as well as carbonatites from ~540 Ma Fen Complex in Norway (Andersen and Taylor, 1988) and the ~16 Ma Kaiserstuhl Volcanic Complex in Germany (Kraml et al., 2006).

## 3.2 Methods

### 3.2.1 Petrography and geochemical imaging

Petrographic thin sections were prepared (polished to approximately 60 μm thickness) for all samples and examined using a Zeiss SteREO Discovery V12 stereomicroscope coupled with an AxioCam MRc camera. Selected carbonates were additionally analyzed with a Cathodoluminescence (CL) microscope. CL images were acquired with a Cambridge Instruments Citl CCL 8200 Mk3A cold-cathode system linked to a Zeiss Axiolab microscope (operating voltage of approximately 15 kV and electric current of approximately 250-300 μA) and a Zeiss AxioCam 703 camera.

Minerals were identified by their optical characteristics and Raman spectroscopy, using a Horiba Jobin-Yvon LabRam-HR 800 UV spectrometer with a focal length of 800 mm and an excitation wavelength of 488 nm produced by an Argon ion laser (Melles Griot IMA 106020B0S) and with a WITec alpha300 R fibre-coupled ultra-high throughput spectrometer. The former spectrometer was calibrated using a silicon standard with a major peak at 520.4 $cm^{-1}$, and the spectra were processed using software Fityk (Wojdyr, 2010) and comparatively analyzed based on references from the RRUFF database.

Element distributions were mapped using a Bruker M4 Tornado micro-X-ray fluorescence (μXRF) instrument equipped with a XFlash 430 Silicon Drift Detector. Measurements were performed at a voltage of 50 kV and a current of 400 μA with a spot size of 20 μm and a chamber pressure of 20 mbar.

### 3.2.2 Stable carbon and oxygen isotopes ($\delta^{13}C$, $\delta^{18}O$)

For stable isotope analyses, sample chips (diameter ~1 cm) were obtained from pristine areas (i.e., free of visible alteration, inclusions, and secondary porosity) using a microdrill. The sample chips were cleaned three times in ethanol using an ultrasonic bath and dried at room temperature before being crushed into small pieces. Carbonate was then picked out and powdered in an agate mortar and well homogenized. Additionally, some carbonate facies, including carbonate veinlets and carbonate inclusions, were extracted using a drill from individual mineral phases from polished rock slabs.

Carbon and oxygen stable isotopes of the carbonates were measured at 70 °C using a Thermo Scientific Kiel IV carbonate device coupled with a Finnigan DeltaPlus gas isotope mass spectrometer at the Geoscience Center of the Georg-August-Universität Göttingen. All results were normalized as delta values $\delta^{13}C_{carb}$ and $\delta^{18}O_{carb}$ relative to the Vienna PeeDee Belemnite (VPDB) reference standard. The standard deviation is better than 0.03 ‰ for $\delta^{13}C_{carb}$ and 0.05 ‰ for $\delta^{18}O_{carb}$, calculated by multiple measurements of the in-house carbonate standard Solnhofen.

# 4 Results

## 4.1 Interstitial carbonates

### 4.1.1 Host basalts

The host basalts are pillow-shaped, internally subdivided into more crystalline interiors and quenched glassy rims, and commonly locally cut by tectonic fractures (Fig. 2). The interspaces and fractures are filled with carbonate minerals and chert. In most outcrops, the host basalts and interstitial carbonate minerals are weathered, resulting in orange to brownish colors.

Figure 2: Outcrop photos of Archean pillow basalts from the North Pole Dome, Eastern Pilbara Terrane, Western Australia. The pillows consist of relatively unaltered cores surrounded by quenched rims (black arrows), indicating a sub-aquatic formation. Interspaces between pillows are filled with carbonate minerals ("interstitial carbonate"; white arrows). (a) Outcrop of surficially weathered 3.49 Ga North Star Basalt with interspaces filled by Fe-dolomite and chert cement; (b) Outcrop of surficially weathered 3.48 Ga Dresser Formation lacking interstitial calcite due to weathering; (c) Outcrop of surficially weathered 3.47 Ga Mount Ada Basalt with interspaces filled by fibrous isopachous Fe-dolomite (brown colours, due to weathering) and white chert. It is locally cut by deep carbonate veins shown in (d), implying later fluid circulation. (e) Outcrop of little weathered 3.46 Ga Apex Basalt with interspaces filled with pink calcite, basaltic breccia and minor chert. (f) Outcrop of little weathered ~3.35 Ga Euro Basalt with interspaces and fractures filled by pink calcite. The lengths of the brown and blue hammers are ca. 30 cm and ca. 40 cm, respectively. Scale bars are 10 cm in (c) and 20 cm in (d), respectively.

Although the host basalts show secondary mineral assemblages indicative of greenschist metamorphism (calcite + chlorite + anatase + quartz ± pyrite), phenocrysts (i.e., plagioclase and pyroxene) can still be recognized in the basalt interior of the well-preserved samples, e.g. A22 from the Apex Basalt (Figs. 3a, 4a). Notably, the well-preserved basalts exhibit concentric green ophitic-holohyaline interiors and yellow-green quenched margins. In the margins, the size and density of ovoid spherulites and

190    variolites (amygdules) decrease outwards, merging into the glassy zone (Fig. S1a-c). Carbonate minerals are particularly prominent in voids, veins and variolites within alteration zones, as illustrated by μXRF element overlay images of Si, Ca and Mg (Fig. 3b) as well as by calculated Ca mass changes (Fig. S14b; Appendix C). Except for the devitrified volcanic glass, Si is rich in the interior of the pillow basalt but rare in the alteration zones (Figs. 3b, S14), implying a Si loss during basalt carbonatization. Si yielded during this process was likely enriched in fluids, resulting in chert cementation of interstitial

195    carbonates (Fig. 4). The process can be summarized as follows (Eq.1; note that "$CaSiO_3$" refers to calcium silicate minerals):

$$"CaSiO_3" + CO_2 + H_2O \rightarrow "CaSiO_3" + H_2CO_3 \rightarrow CaCO_3 + SiO_2 + H_2O \qquad (Eq.\,1)$$
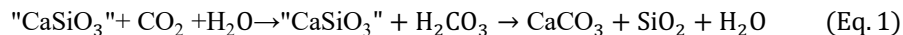
In case of the altered host basalts, progressive deformation and later stage metamorphism are evidenced by the migration and breakup of secondary minerals (e.g. chlorite), erased volcanic textures, as well as by the presence of schistose areas (Figs. 5a, S1d-i). The migration of chlorite, which is a dominant Fe-bearing secondary mineral, caused a loss of Fe in weathered basalts

200    (Fig. 5a). Minerals of the chlorite-group frequently occur in interstitial carbonates close to, and within, tectonic fractures in the pillow basalts (Fig. 5b).
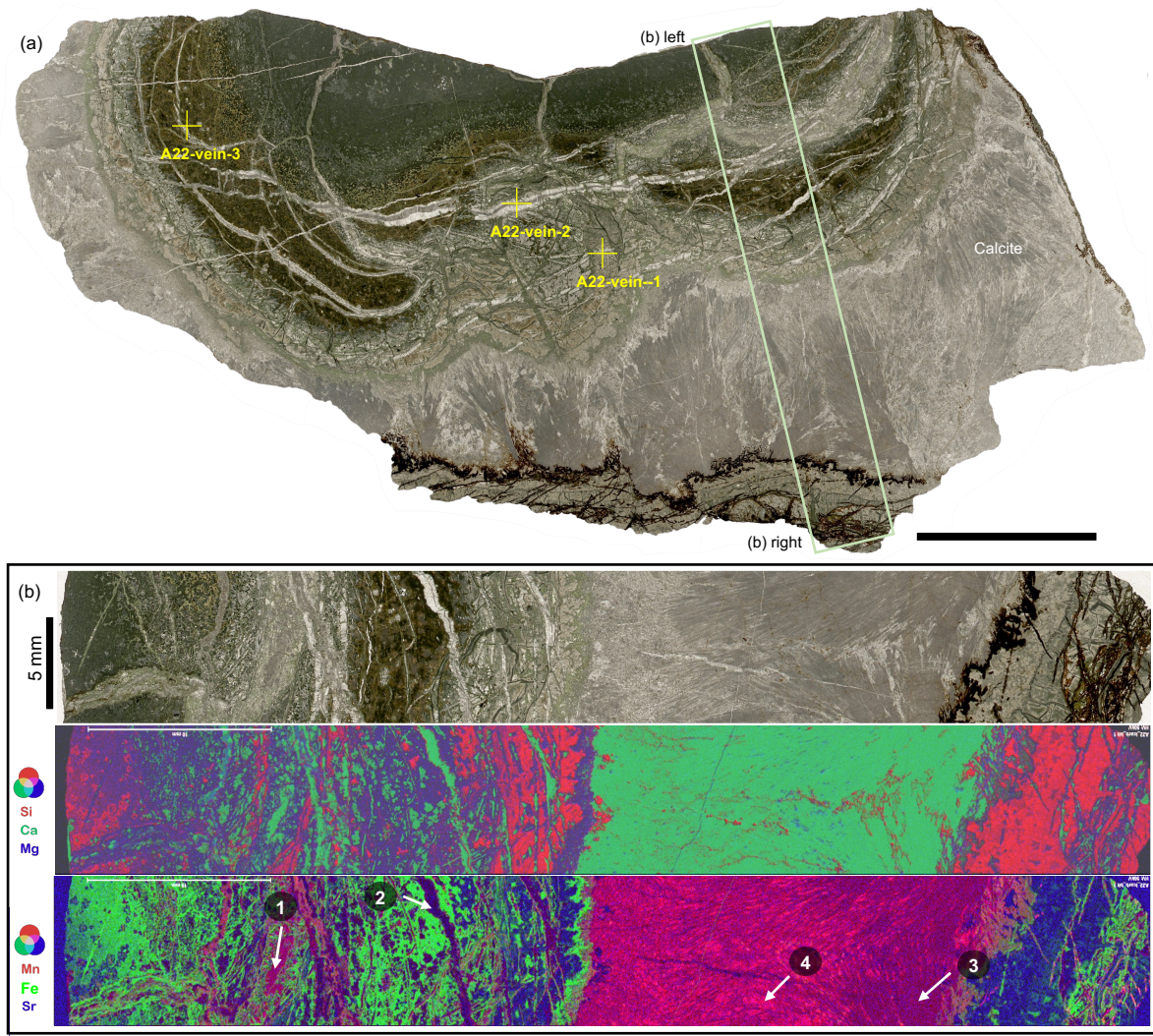
**Figure 3: (a) Thin section scan image (transmitted light) of sample A22 from the Apex Basalt, showing concentric pillow structures of the basalt and well-preserved primary acicular crystal-fans of interstitial carbonates (mainly calcite). Yellow crosses mark the positions of subsamples analysed for stable oxygen and carbon isotopes (Table 1, Fig. S3). The scale bar in (a) is 20 mm. (b) Blow-up image and μXRF mappings of rectangle area highlighted in (a). The false-colour overlapping image of Si (red), Ca (green) and Mg (blue) in the middle panel is well in line with interspaces dominantly filled by calcite with minor chert. In addition, the quenched margin of the basalt seems to be relatively depleted in Si as compared to the core, implying a loss of Si during carbonatization processes (see Eq. 1). The Si yielded by carbonatization was likely enriched in fluids and resulted in the later cementation of interstitial calcite by chert. The false-colour overlapping image of Mn (red), Fe (green) and Sr (blue) in the lower panel highlights the presence of four calcite facies, that is, Mn-enriched syngenetic veins (white arrow 1), Mn-depleted later veins (white arrow 2), Mn-depleted acicular interstitial calcite (white arrow 3), and Mn-enriched calcite cement (white arrow 4). The images of each element are shown in Fig. S5.**
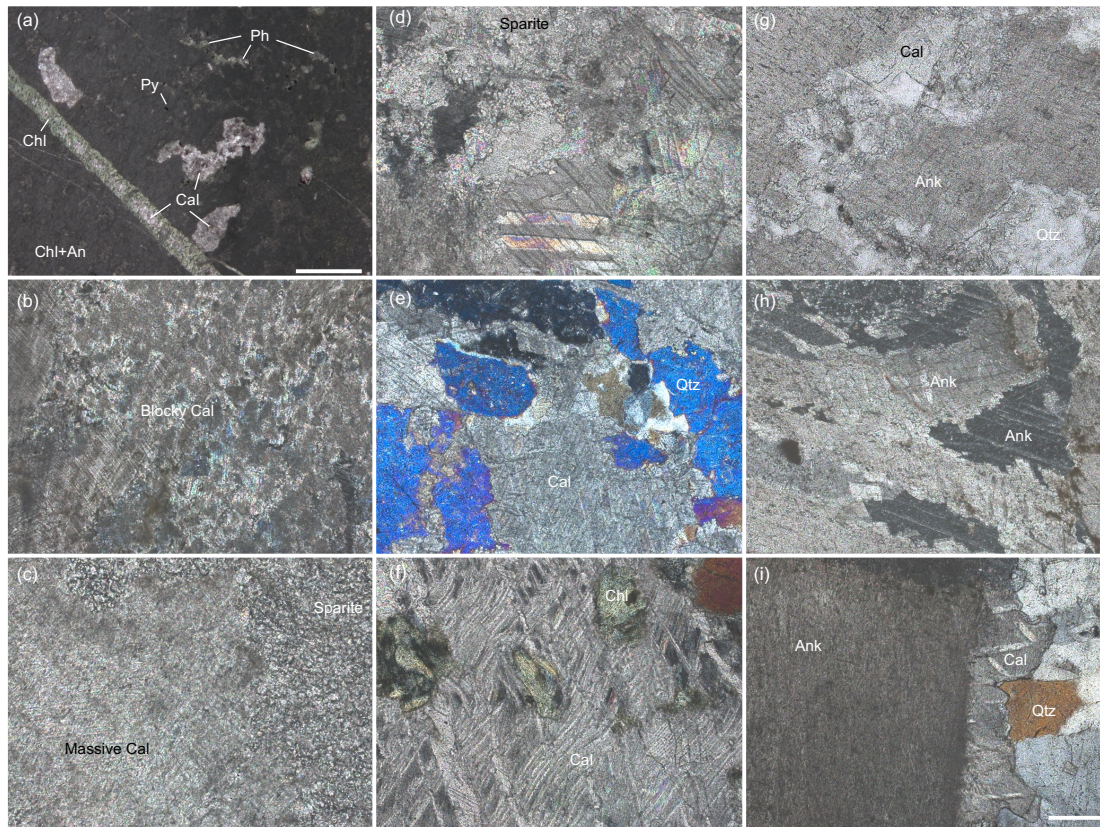
Figure 4: Thin section photographs of altered interstitial carbonates from the North Pole Dome, Eastern Pilbara Terrane, Western Australia. (a) Phenocrysts can be recognized in the well-preserved host basalt, although the secondary mineral assemblage is indicative of greenschist metamorphism (calcite + chlorite + anatase + quartz ± pyrite). The acicular crystal-fan calcite is altered to blocky calcite (b) as well as to massive and sparitic calcite (c). (d) Large sparitic crystals in a wide fracture. (e) The blocky calcites are cemented by quartz. (f) Metamorphic S-C fabrics of sparite and chlorite crystals indicate dynamic metamorphism. (g) Blocky ankerites often show calcite overgrowths at their edges. (h) Some ankerites exhibit features formed by recrystallization and neomorphism. (i) Along dewatering cracks, ankerites in deep carbonate veins are commonly overgrown by calcite and chert cement. (a) to (c): Apex Basalt; (d): Dresser Formation; (e) and (f): Euro Basalt; (g) to (i): Mount Ada Basalt. All photos except (g) were taken under cross-polarized light. Scale bar in (i) corresponds to 200 µm and is applicable to all photographs. Abbreviations: Ph-phenocryst, Cal-calcite, Chl- chlorite, Qtz- quartz, Ank-ankerite.

225
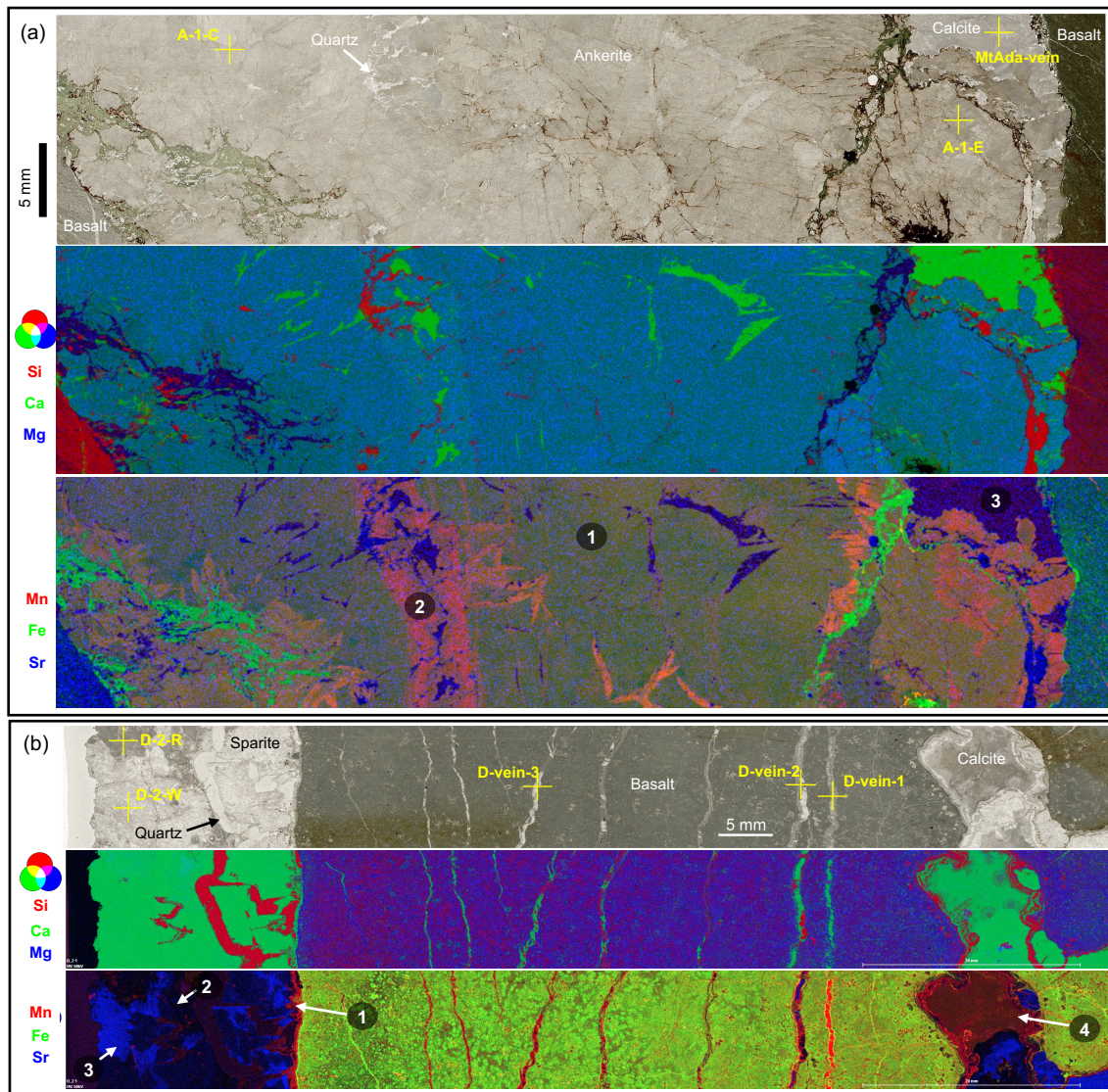
**Figure 5: Thin section scan images (transmitted light) and false-colour overlapping images of elements of interstitial carbonates in (a) the Mount Ada Basalt and (b) the Dresser Formation. (a) Interstitial carbonate in the Mount Ada Basalt consists of blocky and massive ankerite with minor calcite overgrowth and infilling quartz, as evidenced by Fig. S4b and Si (red), Ca (green) and Mg (blue) distributions shown in false-colour overlapping images (middle panel in a). False-colour overlapping images of Mn (red), Fe (green) and Sr (blue) (lower panel in a) highlight the presence of Mn-enriched ankerite (close to metabasalt; number 2 in the figure), Mn-depleted calcite (in later vein; number 3), and ankerite with intermediate enrichments of Mn (distant to metabasalt; number 1). Mn-enriched ankerite might be influenced by later fluids as indicated by calcite and quartz. (b) Interstitial carbonates in the Dresser Formation includes precipitates enriched in Mn (first and fourth generations, shown in the figure by the numbers and arrows), depleted in Mn and Sr (second generation), as well as Mn-depleted but Sr-enriched precipitates (third generation). Precipitates of**

230

235 **the first and fourth generation seem identical to calcite occurring within parallel fractures of basalts, implying precipitation from similar fluids that derived from fluid-basalt reactions. The second and third generation are distinctive from the aforementioned generations, indicating a different origin of the later fluids. Yellow crosses mark the positions of subsamples analysed for stable oxygen and carbon isotopes (Table 1, Fig. S3). The images of each element are shown in Figs. S6, S7.**

### 4.1.2 Primary carbonate phases

240 The primary mineral phase of interstitial carbonates is calcite. Acicular crystal-fans of calcite are only preserved in some samples from the Apex Basalt, but are reduced or absent in most other cases. The terminal tips of the acicular crystal-fans are partly recrystallized to sparitic calcite crystals (Fig. 4b). Microcrystalline ankerite is rarely observed at the basalt margin, mixing with microcrystalline quartz, chlorite, and anatase particles (~nm) (Figs. S2a, S4a). Minor chert locally infills the intercrystalline space of sparite and crystal-fan calcite. Primary carbonates occurring within basalts include blocky calcite in

245 concentric syngenetic veins and fibrous isopachous calcite in tectonic fractures, often showing shear bending through dynamic crystallization (Fig. S2b, e).

Calcite is the dominant primary carbonate phase in all samples, which is in line with the spatially independent distributions of Ca, Mg and Si in the precipitates (Fig. 3b). However, distinct calcite phases show different contents of Mn, with acicular crystal-fan and fibrous isopachous precipitates being depleted in Mn relative to the associated intercrystalline calcites. Fe, Si

250 and Mg are pervasive in basalt and fractures, which is due to the presence of chlorite group minerals (Fig. 5a).

### 4.1.3 Secondary carbonate facies

In many cases, primary interstitial calcite was affected by post-depositional alteration processes such as recrystallization and ankeritization. Recrystallization is widespread, involving the transformation of acicular crystal-fan calcite to inequigranular, blocky, massive, and sparry calcite (Fig. 4b–d). The recrystallized interstitial calcite is commonly cemented by quartz (Fig. 4e,

255 g). In some samples, sparite exhibits a S-C fabric (Fig. 4f), indicative of deformation through dynamic metamorphism in a shear zone (Lister and Snoke, 1984). Noteworthy, sparite in sample D-2 from the Dresser Formation is rather associated with tectonic fractures than with basalt interspaces (Figs. 4d, S2 d-f; Xiang, 2023); therefore, it will be addressed as "fracture-filling calcite" in the following.

Carbonates from the Mount Ada Basalt underwent significant ankeritization, as indicated by abundant blocky and massive

260 ankerite cemented by quartz (Fig. 4g). Rarely observed relict structures "floating" in ankerite evidence acicular crystal-fan calcite as precursor (Fig. S2c). The interstitial ankerite locally underwent recrystallization and neomorphism (Fig. 4h). Calcite veins locally cut the interstitial ankerite and the host basalt. Ankerite precipitates in those samples are commonly overgrown by calcite (Fig. 4g, i).

The secondary carbonates are either Mn- or Sr-enriched (Fig. 5), indicating the influence of at least two diagenetic fluids

265 during later alteration. Secondary Mn-enriched carbonates include recrystallized interstitial calcites and ankerites as well as calcite cements within basalt fractures. Notably, the degree of Mn-enrichment in interstitial ankerites varies, with those formed

through recrystallization and neomorphism or closer to the basaltic parts being relatively more enriched (Fig. 5a). At the same time, calcites overgrowing interstitial ankerites and, even more so, within fractures are enriched in Sr (Fig. 5).

### 4.1.4 $\delta^{13}$C and $\delta^{18}$O values of interstitial carbonates

270    The interstitial carbonates (including both, calcite and ankerite) show $\delta^{13}$C values ranging from -2.37 to +0.99 ‰ (mean = 0.22 ± 0.98 ‰) and $\delta^{18}$O values ranging from -19.81 to -14.34 ‰ (mean = -17.57 ± 1.51 ‰) (Table 1). The fracture-filling calcites exhibit $\delta^{13}$C values ranging from 2.03 to 2.34 ‰ (mean = 2.19 ± 0.13 ‰) and $\delta^{18}$O values ranging from -17.91 to -13.03 ‰ (mean = -15.70 ± 2.53 ‰) (Table 1). Carbonates in veins (see Figs. 3, 5) have the slightly lower $\delta^{13}$C and $\delta^{18}$O values than interstitial carbonates in the same samples (Table 1, Fig. S3).

275    **Table 1: Stable carbon and oxygen isotopic compositions of the early Archean carbonates**

| Lithology | Mineralogy | Formation | Age (Ma) | SampleID | $\delta^{13}$C$_{VPDB}$ (‰) | s.d. | $\delta^{18}$O$_{VSMOW}$ (‰) | s.d. | $\delta^{18}$O$_{VPDB}$ (‰) |
|---|---|---|---|---|---|---|---|---|---|
| Interstitial Carb. | Calcite | Euro Basalt | 3350 | E-1 | 0.21 | 0.03 | 11.08 | 0.05 | -19.23 |
| | | | | E-2 | 0.99 | 0.03 | 10.78 | 0.05 | -19.52 |
| | | | | E-3 | -2.37 | 0.03 | 11.00 | 0.05 | -19.31 |
| | | Apex Basalt | 3460 | A14673-1 | 0.62 | 0.03 | 13.65 | 0.05 | -16.74 |
| | | | | A22-1 | 0.44 | 0.03 | 13.09 | 0.05 | -17.29 |
| | | | | A22-2 | 0.69 | 0.03 | 13.67 | 0.05 | -16.72 |
| | | | | ABAS-1 | 0.65 | 0.03 | 13.41 | 0.05 | -16.97 |
| | | | | ABAS-1 | 0.77 | 0.03 | 14.63 | 0.05 | -15.79 |
| | | | | Apex-1 | 0.25 | 0.03 | 12.79 | 0.05 | -17.58 |
| | | | | Apex-2 | 0.04 | 0.03 | 12.66 | 0.05 | -17.70 |
| | | | | Apex-3 | 0.21 | 0.03 | 13.00 | 0.05 | -17.37 |
| | Ankerite, calcite | Mt.Ada Basalt | 3470 | MtAda-1-C | 0.83 | 0.00 | 12.21 | 0.03 | -18.14 |
| | | | | MtAda-1-E | 0.77 | 0.03 | 11.77 | 0.05 | -18.57 |
| | | | | MtAda-2 | 0.52 | 0.03 | 14.36 | 0.03 | -16.05 |
| | Calcite | Dresser Fm. | 3480 | D-1 | 0.97 | 0.03 | 14.46 | 0.05 | -15.95 |
| | | | | D-3 | 0.63 | 0.03 | 10.49 | 0.05 | -19.81 |
| | | North Star Basalt | 3490 | CP-1 | -2.31 | 0.03 | 11.14 | 0.05 | -19.17 |
| | | | | CP-2 | 0.01 | 0.03 | 16.12 | 0.05 | -14.34 |
| Fracture Carb. | Calcite | Dresser Fm. | 3480 | D-2-IC-1 | 2.03 | 0.03 | 12.45 | 0.03 | -17.91 |
| | | | | D-2-IC-2 | 2.17 | 0.03 | 16.43 | 0.03 | -14.04 |
| | | | | D-2-R | 2.34 | 0.03 | 12.54 | 0.05 | -17.81 |
| | | | | D-2-W | 2.20 | 0.03 | 17.47 | 0.05 | -13.03 |
| Veinlet Carb. | Calcite | Apex Basalt | 3460 | A22-vein-1 | 0.12 | 0.03 | 13.50 | 0.05 | -16.88 |
| | | | | A22-vein-2 | -0.14 | 0.03 | 13.31 | 0.05 | -17.07 |
| | | | | A22-vein-3 | -0.02 | 0.03 | 13.29 | 0.05 | -17.09 |

| Type | Mineral | Formation | Age | Sample | | | | | |
|---|---|---|---|---|---|---|---|---|---|
| | | Mt.Ada Basalt | 3470 | MtAda-1-vein | 0.47 | 0.03 | 10.47 | 0.05 | -19.82 |
| | | Dresser Fm. | 3480 | D-2-vein-1 | -3.77 | 0.03 | 11.30 | 0.05 | -19.02 |
| | | | | D-2-vein-2 | -2.35 | 0.03 | 11.25 | 0.05 | -19.06 |
| | | | | D-2-vein-3 | -1.69 | 0.03 | 11.36 | 0.05 | -18.96 |
| Sed. Carb. | Ankerite | Euro Basalt | 3350 | E-4 | 1.88 | 0.00 | 15.24 | 0.03 | -15.19 |
| | Dolomite | Strelley Pool Fm. | 3410 | JR-Shaw-1 | 2.08 | | 15.01 | | -15.42 |
| | | | 3410 | JR-Shaw-2 | 2.52 | | 15.24 | | -15.20 |
| | | | 3410 | JR-Shaw-3 | 2.55 | | 15.31 | | -15.13 |
| | Ankerite | Dresser Fm. | 3480 | PDP | 1.26 | 0.03 | 17.83 | 0.05 | -12.69 |
| | | | | JR-TSU-1 | 2.24 | | 17.53 | | -12.98 |
| | | | | JR-TSU-2 | 2.22 | | 16.36 | | -14.11 |
| | | | | JR-TSU-3 | 2.17 | | 16.71 | | -13.77 |
| | | | | JR-TSU-4 | 1.61 | | 16.53 | | -13.95 |
| | | | | JR-TSU-5 | 2.24 | | 17.68 | | -12.83 |
| | | | | JR-TSU-6 | 2.54 | | 18.74 | | -11.80 |
| | | | | JR-TSU-7 | 2.42 | | 18.30 | | -12.23 |
| | | | | JR-TSU-8 | 2.34 | 0.05 | 18.43 | 0.07 | -12.10 |
| | | | | JR-TSU-9 | 1.21 | 0.05 | 27.10 | 0.07 | -3.69 |
| | | | | JR-TSU-10 | 1.34 | 0.05 | 15.93 | 0.07 | -14.53 |
| | | | | JR-TSU-11 | 1.61 | | 15.82 | | -14.63 |
| | | | | JR-TSU-12 | 1.61 | | 15.96 | | -14.50 |
| | | | | JR-TSU-13 | 1.49 | | 15.74 | | -14.71 |
| | | | | JR-TSU-14 | 1.38 | | 21.45 | | -9.17 |
| | | | | JR-TSU-15 | 1.10 | | 22.60 | | -8.06 |
| | | | | JR-TSU-16 | 1.78 | | 23.37 | | -7.31 |
| | | | | TSU | 1.46 | 0.03 | 15.80 | 0.05 | -14.66 |
| Sed. Carb. DB | Dolomite, calcite | | | DB | -5.10 | 0.03 | 22.79 | 0.05 | -7.88 |
| | | | | JR-Dress-1 | -5.38 | | 20.54 | | -10.05 |
| | | | | JR-Dress-2 | -6.72 | | 20.19 | | -10.40 |
| | | | | JR-Dress-3 | -6.38 | | 19.81 | | -10.77 |
| | | | | JR-Dress-4 | -6.22 | | 19.70 | | -10.87 |
| | | | | JR-Dress-5 | -6.01 | | 19.94 | | -10.64 |
| | | | | JR-Dress-6 | -4.25 | | 19.24 | | -11.32 |
| | | | | JR-Dress-7 | -5.96 | 1.72 | 1.25 | 4.76 | -28.77 |
| | | | | JR-Dress-8 | -8.07 | 0.34 | 10.50 | 1.30 | -19.79 |
| | | | | JR-Dress-9 | -3.15 | 0.07 | 19.93 | 0.15 | -10.65 |
| Stromatolite | Dolomite | Strelley Pool Fm. | 3410 | Strelley | 2.50 | 0.00 | 17.34 | 0.03 | -13.16 |
| | | | | JR-Strell-1 | 2.46 | | 13.92 | | -16.48 |
| | | | | JR-Strell-2 | 3.28 | | 15.01 | | -15.42 |

| | | | | | | | | | |
|---|---|---|---|---|---|---|---|---|---|
| | | | | JR-Strell-3 | 3.38 | | 14.84 | | -15.59 |
| | | | | JR-Strell-4 | 3.32 | 0.01 | 16.64 | 0.02 | -13.84 |
| | | | | JR-Strell-5 | 2.69 | 0.01 | 15.74 | 0.03 | -14.71 |
| | | | | JR-Strell-6 | 3.30 | 0.01 | 16.56 | 0.02 | -13.92 |
| | | | | JR-Strell-7 | 3.33 | 0.01 | 16.66 | 0.02 | -13.82 |
| | | | | JR-Strell-8 | 2.58 | 0.01 | 15.91 | 0.02 | -14.55 |
| | | | | JR-Strell-9 | 3.21 | 0.01 | 16.68 | 0.03 | -13.80 |
| | | | | JR-Strell-10 | 3.38 | 0.03 | 17.47 | 0.05 | -13.04 |
| | | | | JR-Strell-11 | 3.15 | 0.01 | 16.56 | 0.02 | -13.92 |
| | | | | JR-Strell-12 | 3.19 | 0.01 | 16.63 | 0.02 | -13.84 |
| | | | | JR-Strell-13 | 3.14 | 0.02 | 16.66 | 0.03 | -13.82 |
| | | | | JR-Strell-14 | 3.03 | 0.02 | 18.34 | 0.03 | -12.19 |
| | | | | JR-Strell-15 | 3.05 | 0.01 | 16.77 | 0.02 | -13.71 |
| | | | | JR-Strell-16 | 3.26 | 0.01 | 16.84 | 0.02 | -13.65 |
| | | | | JR-Strell-17 | 3.31 | 0.01 | 16.70 | 0.03 | -13.78 |
| | | | | JR-Strell-18 | 3.04 | 0.01 | 17.17 | 0.01 | -13.33 |
| Stromatolite? | Ankerite, calcite | Isua Supracrustal Belt | 3700 | IS12-1 | 2.35 | 0.08 | 18.80 | 0.11 | -11.74 |
| | | | | IS12-2 | 1.21 | 0.08 | 19.69 | 0.11 | -10.88 |
| | | | | IS12-3 | 1.18 | 0.08 | 19.57 | 0.11 | -11.00 |
| | | | | IS12-4 | 1.11 | 0.08 | 19.59 | 0.11 | -10.98 |
| | | | | IS12-5 | 1.18 | 0.13 | 19.36 | 0.18 | -11.20 |
| | | | | IS12-6 | 1.27 | 0.08 | 19.01 | 0.11 | -11.54 |
| | | | | IS12-7 | 0.45 | 0.08 | 16.85 | 0.11 | -13.64 |
| | | | | JR-IS-1 | 0.74 | 0.08 | 19.30 | 0.11 | -11.26 |
| | | | | JR-IS-2 | 0.98 | | 19.23 | | -11.33 |
| | | | | IS-12 | 0.99 | 0.03 | 18.88 | 0.05 | -11.66 |
| | | | | IS-12-C | 1.03 | 0.03 | 19.44 | 0.03 | -11.12 |
| | | | | IS-12-Q | 0.78 | 0.03 | 19.27 | 0.03 | -11.29 |
| Metasomatic Carb. | Dolomite | | | JR-IS9 | -2.11 | | 11.46 | | -18.86 |
| | | | | IS9-1 | -2.37 | 0.08 | 11.64 | 0.11 | -18.69 |
| | | | | IS9-2 | -1.84 | 0.08 | 11.16 | 0.11 | -19.15 |
| | | | | IS9-3 | -1.74 | 0.08 | 10.93 | 0.11 | -19.38 |
| | | | | IS9-4 | -1.93 | 0.08 | 11.49 | 0.11 | -18.83 |
| | | | | IS9-5 | -2.03 | 0.00 | 11.36 | 0.03 | -18.96 |
| Rhodochrosite | Rhodochrosite | Fig Tree Fm. | 3260 | Figtree-1 | -12.74 | | 6.91 | | -23.28 |
| | | | | Figtree-2 | -10.76 | | 12.65 | | -17.71 |
| | | | | Figtree-3 | -19.34 | | -4.93 | | -34.76 |
| | | | | Figtree-4 | -12.12 | | 5.90 | | -24.26 |
| | | | | Figtree-5 | -18.23 | | -6.85 | | -36.62 |
| | | | | Figtree-6 | -23.00 | | -12.32 | | -41.93 |

| Carb. in barite | Dolomite, calcite, strontianite | Dresser Fm. | 3480 | JR-DressBart-1 | | | | | |
|---|---|---|---|---|---|---|---|---|---|
| | | | | | -18.14 | 0.20 | 9.37 | 0.50 | -20.89 |
| | | | | JR-DressBart-2 | -18.46 | 0.20 | 10.47 | 0.50 | -19.82 |
| | | | | JR-DressBart-3 | -11.37 | 0.20 | 11.32 | 0.50 | -19.00 |
| | | | | JR-DressBart-4 | -15.95 | 0.20 | 9.92 | 0.50 | -20.36 |
| | | | | JR-DressBart-5 | -11.07 | 0.20 | 10.81 | 0.50 | -19.49 |
| | | | | JR-DressBart-6 | -15.09 | 0.05 | 11.51 | 0.07 | -18.82 |
| | | | | JR-DressBart-7 | -11.81 | 0.10 | 12.06 | 0.30 | -18.28 |
| | | | | JR-DressBart-8 | -12.40 | 0.10 | 13.78 | 0.30 | -16.61 |
| | | | | JR-DressBart-9 | -9.79 | 0.10 | 12.85 | 0.30 | -17.52 |
| | | | | JR-DressBart-10 | -14.53 | 0.10 | 12.03 | 0.30 | -18.31 |
| | | | | JR-DressBart-11 | -11.20 | 0.20 | 12.30 | 0.50 | -18.05 |
| | | | | JR-DressBart-12 | -2.70 | 0.20 | 14.00 | 0.50 | -16.40 |
| | | | | JR-DressBart-13 | -10.83 | 0.10 | 12.54 | 0.30 | -17.82 |
| Carbonatite | Calcite | | | JR-C1 | -4.91 | | 7.13 | | -23.07 |
| | | | | JR-C2 | -5.84 | | 7.13 | | -23.06 |
| | | | | JR-C3 | -5.91 | | 7.00 | | -23.19 |
| | | | | JR-C4 | -3.29 | | 18.35 | | -12.18 |

**Note:**

1. $\delta^{18}O_{VPDB}=0.970017*\delta^{18}O_{VSMOW} -29.98$ (Coplen, 1988)
2. s.d. is the standard deviation calculated by multiple measurements of the in-house carbonate standard Solnhofen.
3. Abbreviations: Fm.- Formation , Mt.-Mount, Sed.-sedimentary, Carb. –carbonate;
4. The question mark in "Stromatolite (?)" indicates its controversial origin.
5. "Carb. in barite" refers to carbonate inclusions in bladed black barite.

## 4.2 Sedimentary carbonates

### 4.2.1 Laminated micritic carbonates

Laminated micritic carbonate occurs in a ca. 5 m thick sedimentary succession (Fig. 6a, b) interbedded with pillow basalts of the Dresser Formation (Fig. 2b). The micritic carbonate is predominantly brownish and finely bedded. The association with pillow basalts indicates an interval of generally quiet-water sedimentation, although the succession might preserve the oldest record of a tsunami event on Earth (Runge et al. 2022).
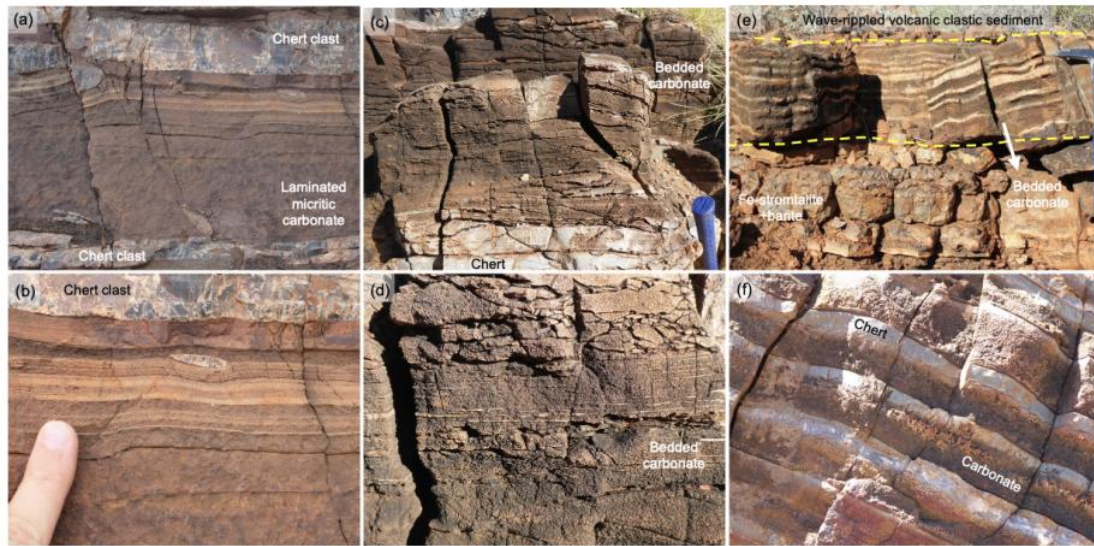
**Figure 6: Outcrop photos of the bedded sedimentary carbonates from the North Pole Dome in the East Pilbara Terrane, Western Australia. (a, b) Laminated micritic sedimentary carbonate of Dresser Formation, the potential oldest reported tsunami deposit (Runge et al., 2022). (c, d) Finely bedded carbonate rock overlying the 3.35 Ga Euro Basalt. The shown bed is 10 cm thick. (e, f) Interlayered carbonate-chert beds (7 to 11 beds between the yellow dashed line) of Dresser Formation. This unit is overlain by wave rippled volcanic clastic sediment with remains of evaporitic minerals and organic films on top, while the underlying rock is bedded barite with sulfidic stromatolites atop. The length of hammer is ca. 40 cm.**

The laminated micritic carbonate consists of fine-grained carbonate crystals with abundant organic clots and flakes (Fig. 7a), and locally euhedral and subhedral carbonate rhombs that have a cloudy center and clear rim enveloped by organic matter (Fig. 7b). *In situ* geochemical mappings and Raman spectra (Fig. 7c, S8; Xiang, 2023) indicate that the carbonate crystals are Mn-enriched ankerite, while that the cloudy centers consist of organic matter. Calculated Raman-based temperatures (based on Lünsdorf et al., 2017) of ~ 300–350 °C agree well with the peak metamorphic temperatures of this region (Allwood et al., 2006b; Hickman and Van Kranendonk, 2012a; Van Kranendonk et al., 2019a). The laminae are caused by changing crystal sizes and organic matter contents, with finer-grain sizes and higher organic matter contents resulting in darker colors. A similar bedded micritic carbonate is observed in samples from drilling core PDP2c (see Van Kranendonk et al., 2019b).
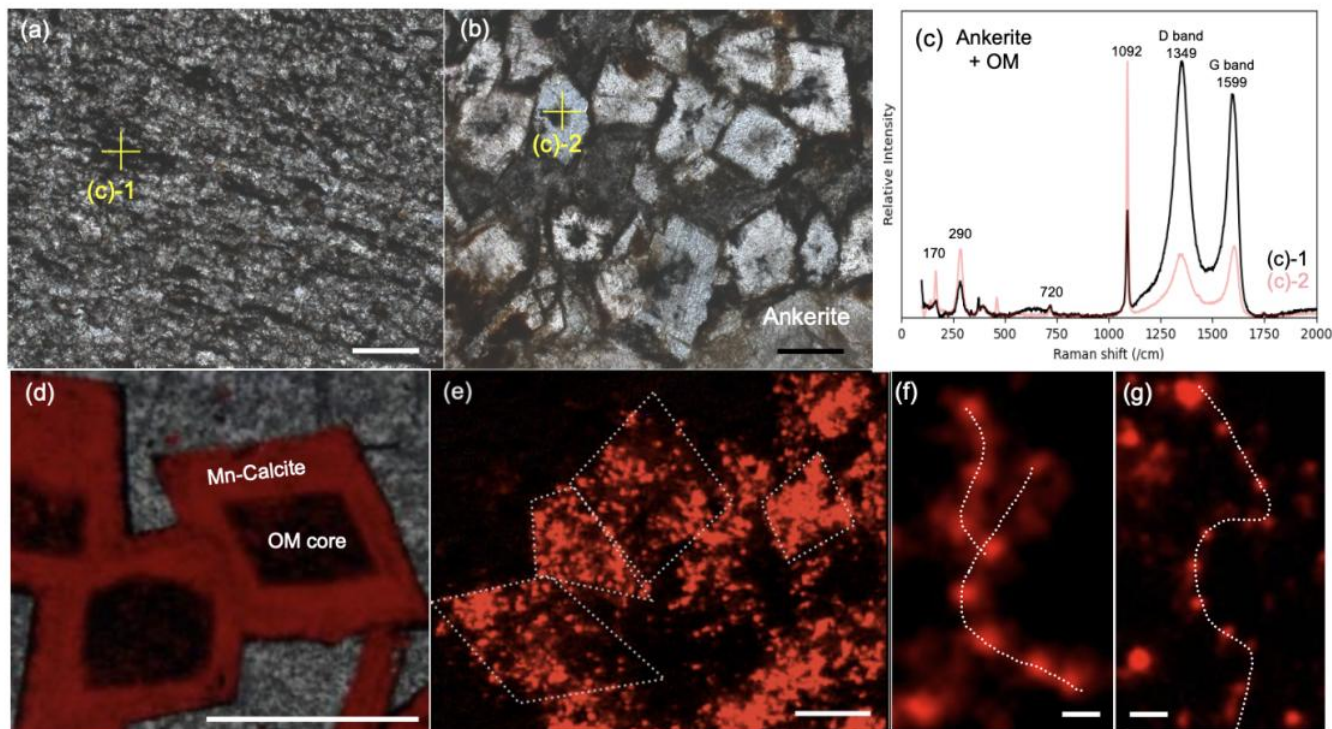
**Figure 7: Spatial relationships between sedimentary carbonates and organic matter. (a) Interbed of the laminated micritic carbonate containing flakes and clots of organic material (OM). (b) Euhedral and subhedral carbonate rhombs, exhibiting organic matter in their cores and at their outer edges. (c) Raman spectra for spots in (a) and (b), supporting the presence of ankerite and organic matter. (d) Euhedral calcite rhombs with cores of organic matter are cemented by chert. (e) Close-up view of calcite rhombs showing Mn-enriched dolomite particles within the calcite crust (some crystals are indicated by dotted lines). (f, g) Arrangements of Mn-enriched dolomite particles that somewhat resemble kutnahorite formed by *Idiomarina loihiensis* strains (Rincón-Tomás et al., 2016). (a) and (b) were taken under plane-polarized light. The scale bar in (f) and (g) are 5 μm, while all others are 200 μm).**

### 4.2.2 Bedded chert-carbonates

The bedded chert-carbonates are characterized by carbonate-chert couples and occur at the top of a chert layer from the Euro Basalt as well as in the Dresser Formation ("Euro bedded carbonate" and "Dresser bedded carbonate" in the following) (Fig. 6). The Dresser bedded carbonate consists of 9–11 carbonate-chert couplets with radiating crystal splays. Because of its distinct appearance, it was previously named "zebra rock" (Hickman and Van Kranendonk, 2012b; see Van Kranendonk et al. 2019b for a detailed description). Notably, it occurs between a unit of sulfidic stromatolites and bladed barite below, and wave rippled volcanoclastic sediments above (Fig. 6e).

Individual carbonate-chert couplets consist of fining-upward successions of euhedral to subhedral carbonate rhombs in a chert matrix (Fig. 8a, b). In the Dresser bedded carbonate, carbonate rhombs are commonly dolomite and calcite (Fig. S4c), and

320  clusters of radiating carbonate crystal splays occur at the base of each couplet (Figs. 6f, 8a). Some carbonate rhombs have an organic core (Fig. 7d) and show a strong patchy Mn enrichment pattern under CL (Fig. 7e–g), somewhat similar to kutnahorite [Ca(Mn,Mg,Fe)(CO$_3$)$_2$] formed by modern *Idiomarina loihiensis* (ɣ-proteobacteria) (Rincón-Tomás et al., 2016). The euhedral to subhedral carbonate rhombs and the highly porous chert matrix (Fig. 8b) indicate low compaction after deposition. In the Euro bedded carbonate, organic matter is rare and only interbedded between carbonate crystals (ankerite; Fig. S4d, e). Although

325  the Euro bedded carbonate exhibits the repeated grading of ankerite rhombs in a chert matrix, pressure dissolution features associated with ankerite crystals and the nonporous microcrystalline chert matrix imply a stronger post-depositional compaction (Fig. S9a, b).
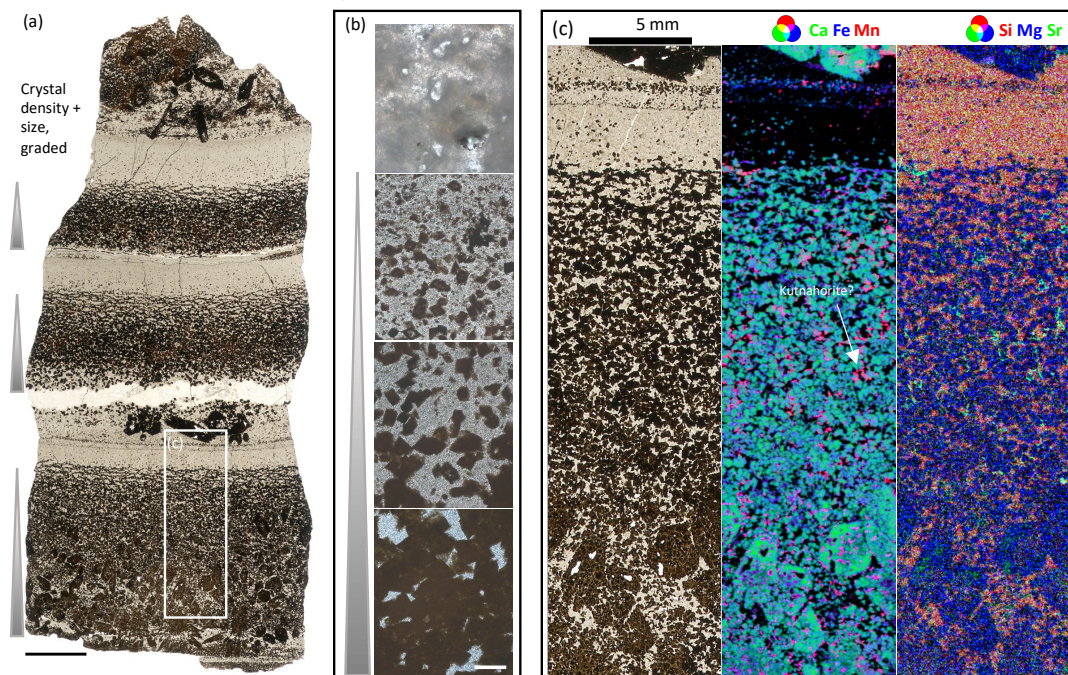
**Figure 8: The bedded sedimentary carbonate-chert rock from Dresser Formation. (a) The scan image (transmitted light) of thin**
330  **section shows repeated graded carbonate layers with the crystal size and density decreasing upwards. One layer is shown discontinuously in (b), that euhedral carbonates grade into the chert layer of high-porosity. The rectangle area is magnified in (c). (c) The false-colour overlapping images show that the Mn-dolomite particles distribute on the edge of calcite crystals. Scale bar in (a) is 10 mm and in (b) is 200 µm. The images of each element are shown in Fig. S10.**

*In situ* geochemical mappings reveal that the Dresser bedded carbonate predominantly consists of Fe-enriched dolomite and
335  calcite with Mn-enriched dolomite particles along its edges (Fig. 8c), in agreement with the observed CL patterns. The Euro Basalt related bedded carbonate comprises Mn-enriched ankerite (Fig. S9).

### 4.2.3 δ¹³C and δ¹⁸O values of sedimentary carbonates

Laminated micritic carbonate and the Euro Basalt related bedded carbonate show δ¹³C values between 1.10 and 2.55 ‰ (mean = 1.85 ± 0.48‰) and δ¹⁸O values between -15.42 and -3.69 ‰ (mean = -12.75 ± 3.00 ‰) (Table 1). The Dresser bedded carbonate, in contrast, exhibits the more negative δ¹³C values ranging from -8.07 to -3.15 ‰ (mean = -5.72 ± 1.36 ‰) and δ¹⁸O values ranging from -28.77 to -7.88 ‰ (mean = -13.11 ± 6.32 ‰) (Table 1).

### 4.3 Stromatolites

The stromatolitic carbonates were located from the second member of the Strelley Pool Formation. Stromatolite morphologies and arguments for biogenicity have been reported in detail elsewhere (Allwood et al., 2006a, 2007; Van Kranendonk et al. 2003; Van Kranendonk, 2011; Duda et al., 2016; Viehmann et al., 2020). Briefly, stromatolites show a high morphological diversity, ranging from coniform and finely laminated to large domical forms, and overly centimeter-sized carbonate fans (Fig. 9).
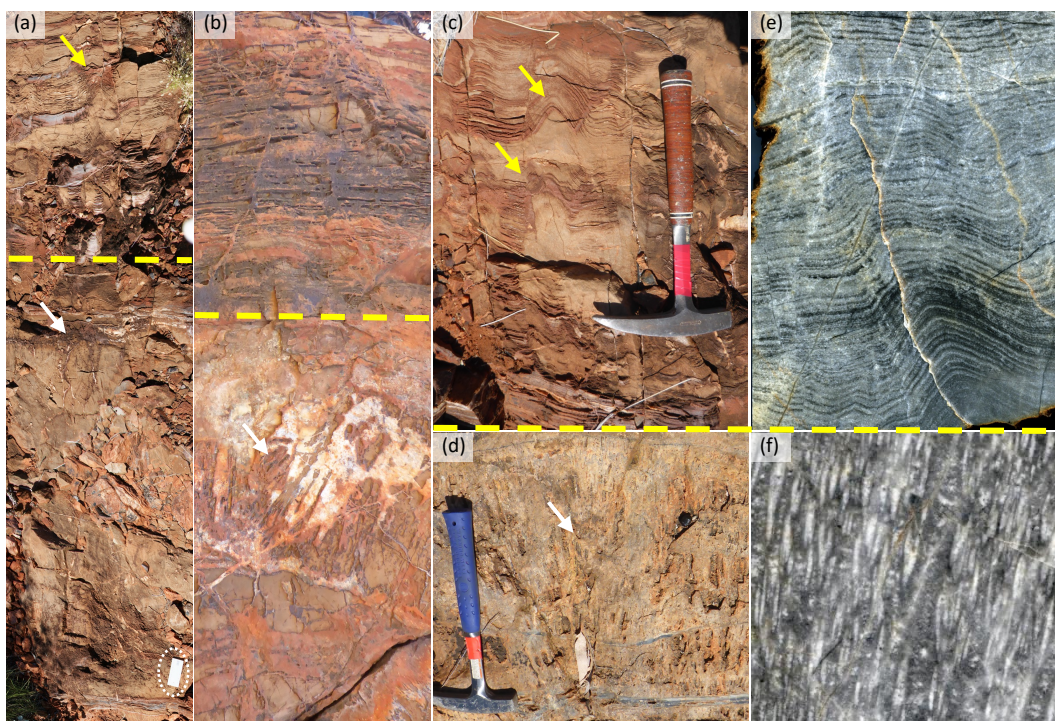
**Figure 9: Photos of stromatolites from the Strelley Pool Formation near the Trendall site in the East Pilbara Terrane, Western Australia. The yellow dashed line marks the boundary between the upper unit with conical stromatolites (yellow arrow) and the lower unit with carbonate fans (white arrow). (a) Composite photo of the outcrop. The ruler (white dotted circle) is 15 cm in length. (b) Close-up view of an outcrop showing the layered stromatolite consisting of carbonate (weathered and partly absent) and chert (dark beds), atop the large carbonate fan on a chert matrix. (c, d) Close-up view of the conical stromatolites (c) and carbonate fans**

**(d). (e, f)** Cross-section views of samples corresponding to (c) and (d), respectively. The length of the brown and blue hammers in (c) and (d) are ~30 cm and ~40 cm, respectively.

The studied sample is a silicified coniform stromatolite with alternating laminae of equigranular anhedral dolomite that often preserves organic matter. The laminae margin contains euhedral dolomite overgrowth (Fig. S4f). Detailed cement stratigraphy involving CL microscopy indicate the presence of at least three dolomite generations (Fig. S11), in line with previous works (Allwood et al., 2009, 2010; Flannery et al., 2018). The stromatolites occur atop large, chert cemented carbonate fans (~ 40 cm) situated on a chert layer (Fig. 9). The carbonate fans encompass fusiform dolomite aggregations (Fig. 9f).

The stromatolites show $\delta^{13}C$ values ranging from 2.46 to 3.38 ‰ (mean = 3.08 ± 0.30 ‰) and $\delta^{18}O$ values ranging from -16.48 to -12.19 ‰ (mean = -14.03 ± 0.98 ‰), consistent with data reported in Lindsay et al. (2005) and Flannery et al. (2018).

## 5 Discussion

### 5.1 Formation pathways of the EPT carbonates

The tectonic model of the EPT involves a volcanic plateau characterized by surface topographical changes, as indicated by pillow basalt successions and shallow water deposits (Smithies et al., 2003, 2005, 2007a, b; Van Kranendonk, 2006; Van Kranendonk et al, 2007a, b, 2019a). Our survey demonstrates that carbonates occur in very different EPT environments, ranging from deep marine settings to terrestrial ponds, which all have been differently influenced by hydrothermal processes.

### 5.1.1 Carbonate abiotically precipitated from hydrothermal fluids

Carbonates associated with Archean pillow basalts are well known from various localities worldwide (Roberts, 1987; Veizer, 1989a, b; Kitajima et al. 2001; Nakamura and Kato, 2004). Today, the formation of such carbonates is triggered by fluctuations in alkalinity, salinity and water temperature (Degens et al., 1984; Kempe, 1990; Reitner et al. 1995b; Flügel, 2010), i.e., the underlying processes are controlled by abiotic parameters. In modern settings, carbonates usually precipitate from low- to moderate-temperature hydrothermal fluids during the latest stage of seafloor alteration (Bach et al., 2001, 2003, 2011; Coogan and Gillis, 2013); as a consequence, they tend to be more abundant in older crusts (Gillis et al., 2001; Heft et al., 2008; Coogan and Gillis, 2013). The precipitation of Ca-Mg-Fe carbonates and formation of silica-bearing fluids linked to basalt-fluid interactions has also been demonstrated by experimental work and numerical simulations (~22 to 350 °C) (Gysi and Stefánsson, 2011; Gudbrandsson et al., 2011; Stockmann et al., 2011; Galeczka et al., 2013a, b, 2014; McGrail et al., 2017; Menefee et al., 2018; Wolff-Boenisch and Galeczka, 2018; Xiong et al., 2018; Voigt et al., 2018).

There is no evidence for a potential biological influence on the formation of EPT basalt-associated carbonates as for instance organic remains. At the same time, precipitation of these carbonates could have been abiotically triggered by infiltration of $CO_2$-enriched seawater and/or basalt-water interactions under hydrothermal conditions, which result in a higher alkalinity and higher cation concentrations (Fig. 10). Indeed, fracture-filling calcite shows the lowest $^{87}Sr/^{86}Sr$ ratio (0.700596) and REE+Y pattern that is considered typical of Archean seawater (Appendix B; for further details see Xiang, 2023), indicating the

385 percolation of seawater-derived $CO_2$-rich fluids through basaltic crust 3.5 Ga ago (Kitajima et al. 2001; Nakamura and Kato, 2002; Yamamoto et al., 2004). In this light, $\delta^{13}C$ signatures of fracture-filling calcites ($2.18 \pm 0.13$ ‰ on average; Fig. 11) may reflect Archean seawater, while $\delta^{13}C$ signatures of interstitial carbonates ($0.22 \pm 0.98$ ‰ on average; Fig. 11) indicate admixture of hydrothermally derived mantle-derived carbon ($\delta^{13}C$ of -5 to -6 ‰; Degens et al. 1984, Hayes and Waldbauer 2006). This is reflected in the common lower $\delta^{13}C$ values of veinlet carbonates than the interstitial carbonates (Fig. S3).

390
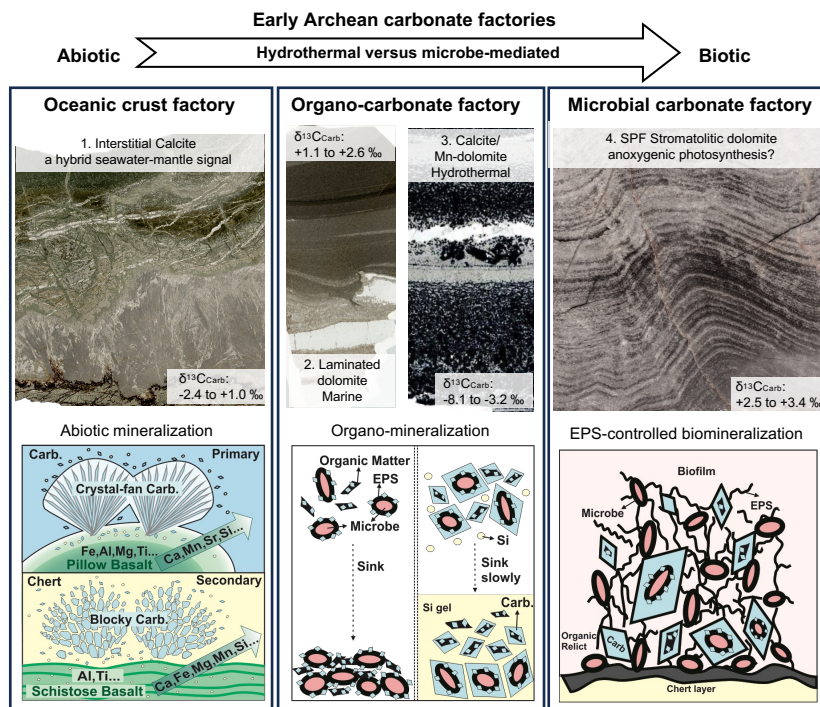
**Figure 10: The lithological features and formation pathways of the three carbonate factories in the early Archean, including an oceanic crust factory, an organo-carbonate factory and a microbial carbonate factory. Carbon precipitation in the oceanic crust factory is an abiotic and inorganic process driven by seawater-basalt interaction, which produce hydrothermal fluids with high carbonate alkalinity and high cation concentrations. Carbonate precipitation in the organo-carbonate factory is linked to organic**
395 **macromolecules (i.e., organo-mineralization). Carbonate precipitation in the microbial carbonate factory occurs through EPS-controlled biomineralization, with anoxygenic photoautotrophs being a likely source of the EPS (adapted from Reitner et al., 2001). (Abbreviations in figure: "Carb.", "Carb"- carbonate; "EPS"- extracellular polymeric substances)**
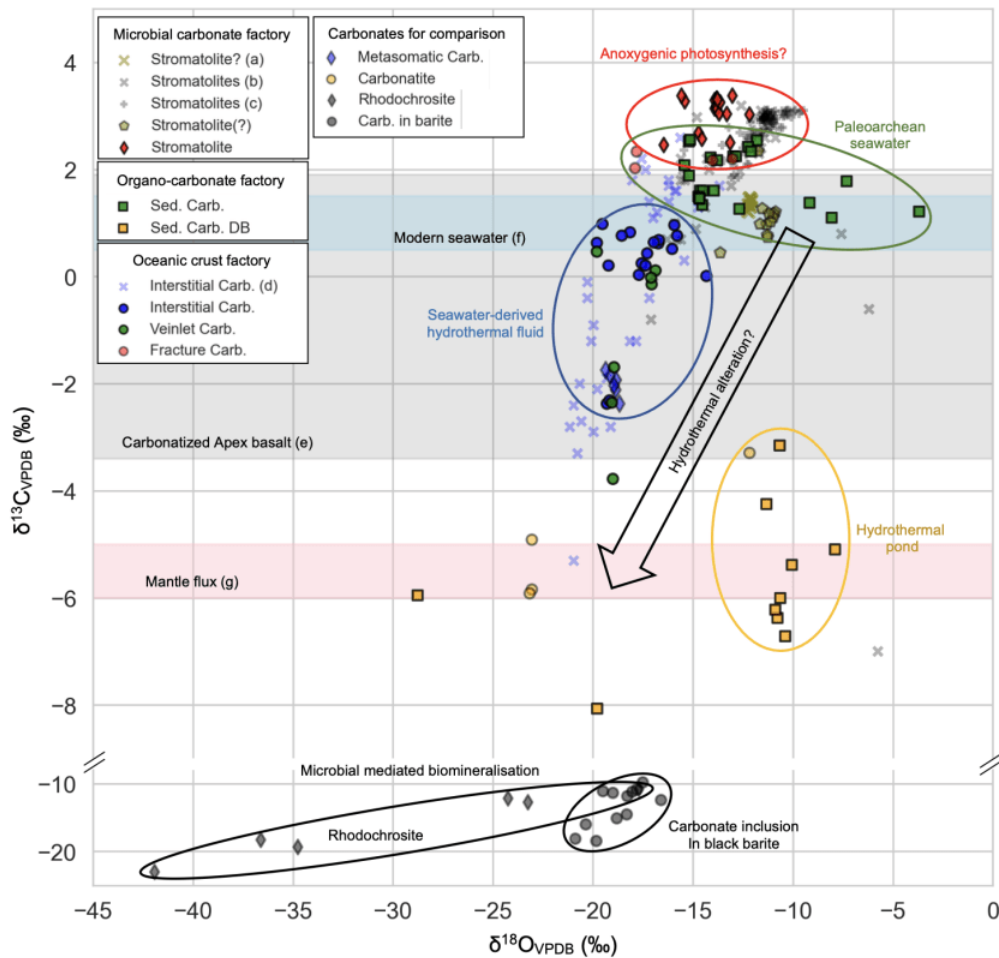
**Figure 11: Stable carbon and oxygen isotopic (δ¹³C, δ¹⁸O) compositions of early Archean carbonates (Carb.). In tendency, δ¹³C and δ¹⁸O values decrease from the stromatolite through marine sedimentary carbonate (Sed. Carb.) to interstitial carbonate, possibly reflecting increasing admixture of mantle-derived carbon. Own data (square, circle, diamond, and pentagon symbols) are given in Table 1. Reference data (including cross and plus symbols) from (a) Nutman et al. (2016), (b) Lindsay et al. (2005), (c) Flannery et al. (2018), (d) Shibuya et al. (2012), (e) Nakamura and Kato (2004), (f) Kroopnick (1980) and Tan (1988), (g) Degens et al. (1984), and Hayes and Waldbauer (2006). Note that "Carb. in barite" indicates carbonate inclusions in black barites from the ~3.5 Ga Dresser Formation (Western Australia), and that question marks in sample labels highlight the controversial biogenicity of the material.**

The mixture of different fluids is also supported by $^{87}Sr/^{86}Sr$ ratios of primary interstitial calcite associated with the Apex basalt (0.703094 ± 0.000979), laying between those of early Archean seawater and Apex pillow basalt (0.700596 and 0.706337 ± 0.000954, respectively; Appendix B; for further details see Xiang, 2023). On the other hand, the precipitation of calcite in vesicles and veins of basalts, as well as the formation of acicular calcite crystal-fans growing at pillow margins (Fig. 3a), could

have been driven by an elevated alkalinity and higher Ca levels, which derived from hydrothermal basalt-water interactions. The observed blocky and massive interstitial calcite or ankerite (Figs. 4, 5) probably resulted from recrystallization and ankeritization of primary calcite precipitates, driven by Mg-, Fe-, Al-, Si-, and Mn-enriched fluids deriving from hydrothermal chlorite breakdown in the basalts (Fig. 3). In summary, carbonates associated with pillowed basalts are inferred to have precipitated abiotically on and below the seafloor (Fig. 12).
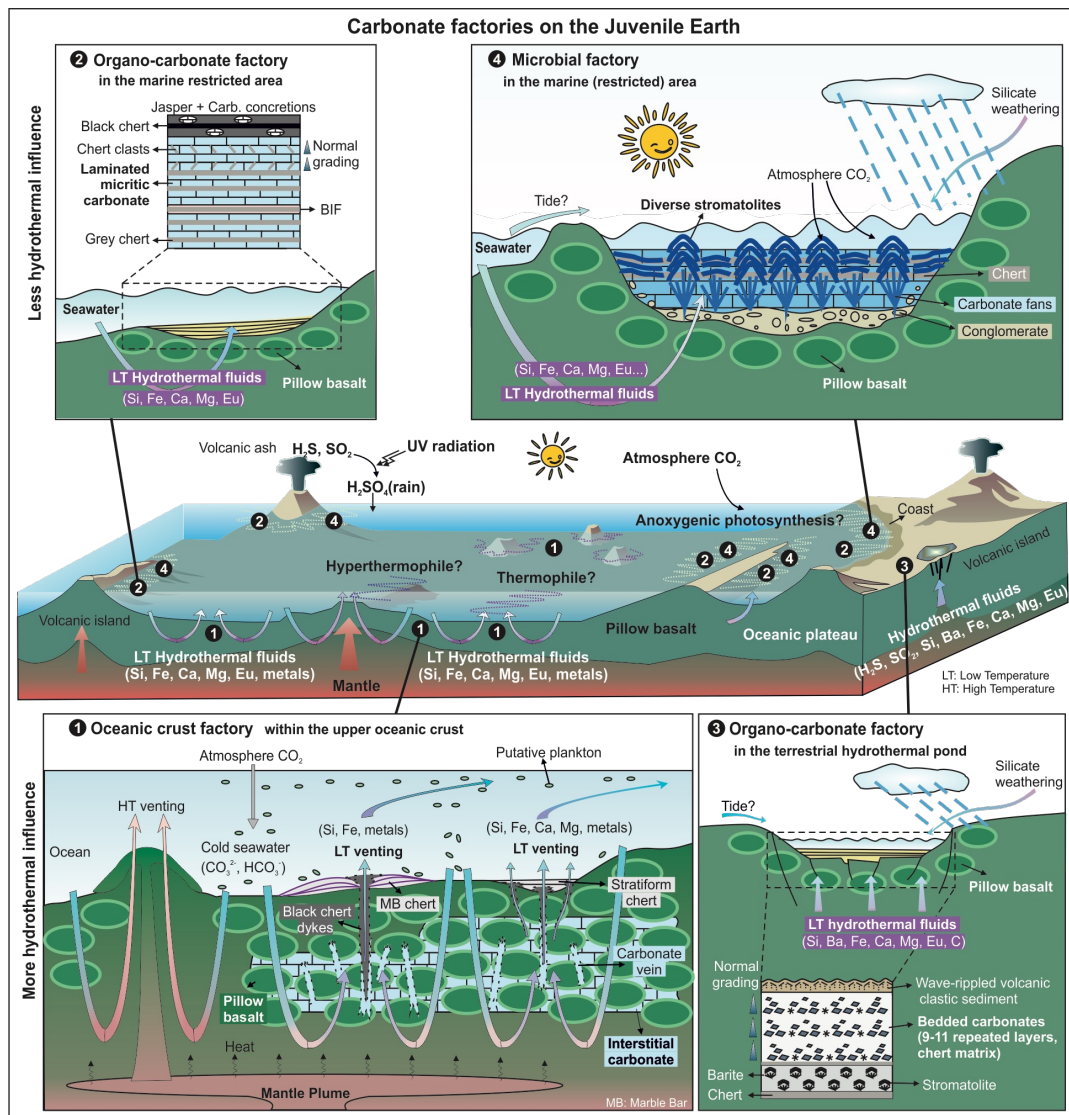
**Figure 12: The possible localities of the three early Archean carbonate factories (adapted from Nisbet and Sleep, 2001; Runge et al., 2022). The oceanic crust factory commonly occurs in deeper marine environments within the upper oceanic crust (number 1). The organo-carbonate factory may operate in diverse environments where organic matter (biotic and/or abiotic) is abundant and fluids are supersaturated in $Ca^{2+}$ and $CO_2$, and which are intermittently influenced by hydrothermal fluids (number 2 and 3). The**

**microbial factory likely forms in photic, relatively restricted, shallow marine environments like lagoons on the slope or platform, with minor detritus and rare hydrothermal inputs (number 4).**

### 5.1.2 Bedded sedimentary carbonates – a product of organo-mineralization

EPT bedded sedimentary carbonate rocks preserve abundant organic remains, for instance occurring as dispersed flakes and
425   clots within micrite (Fig. 7), perhaps indicating a genetic relationship. Organic matrices and compounds inherited from living organisms may retain mineralizing properties (Défarge and Trichet, 1995; Trichet and Défarge, 1995). To distinguish minerals formed through mineralization linked to organic matrices and compounds from those whose formation is induced by living organisms, the terms "organomineral" and "organo-mineralization" were introduced at the 7th International Symposium on Biomineralization in 1995 and further developed in the following decade (Défarge and Trichet, 1995; Reitner et al., 1995b,
430   1997; Arp et al., 1999, 2001, 2003; Neuweiler et al., 1999;Riding, 2000; Pratt, 2001; Reitner, 2004; Gautret and Trichet, 2005), before being finally confirmed in following studies (Perry et al., 2007, 2009; Défarge et al., 2009; Altermann et al., 2009).

Fine-grained carbonates such as micritic calcite or dolomite are typical products of organo-mineralization. Indeed, micrite can form autochthonously (i.e., "automicrite"), involving Ca-binding by aspartic acid- and glutamic acid-rich (briefly, Asp- and
435   Glu-) proteinous macromolecules and negatively charged polysaccharids initiating carbonate crystal nucleation (Reitner et al. 1995a, b, c; Reitner and Neuweiler, 1995; Trichet and Défarge, 1995). It is consequently termed "organomicrite", which is a distinct subset of automicrite (Reitner et al., 1995b). Organomicrites are widespread in Phanerozoic carbonate depositional systems, particularly important in microbial mats and biofilms (Reitner et al., 1995a, b, c; Riding, 2000; Schlager, 2000 2003; Reitner and Thiel, 2011; Reijmer, 2021), as well as in the SPF stromatolites. However, it is important to highlight that organo-
440   mineralization is not restricted to organic matter from biological sources (Défarge et al., 2009); in fact, laboratory experiments indicated that abiotic organic matter as e.g. from the Murchison CM2 meteorite can also mediate carbonate precipitation (Reitner, 2004).

Organomicrites are abundant in some EPT facies. The precipitation and sedimentation of organomicrites result in the finely laminated carbonate deposits (Figs. 7a, 10). However, carbonate precipitation was more complicated in case of fine-graded,
445   bedded chert-carbonates (Figs. 7b-d, 10). In this case, organomicrites can serve as new nucleation centers for the development of euhedral carbonate rhombs. Under low-energy conditions, the fine-grained carbonate crystals precipitate slowly, displaying pronounced normal grading (Figs. 8b, 10). On the other hand, occurrence of Fe/Mn-enriched carbonates and the chert matrix is indicative of involvement of Si-bearing hydrothermal fluids in this process (Fig. 8). Hydrothermal fluids provided significant alkaline metals and silicon. Silicon precipitated as opal-A, a soluble hydrated amorphous silica phase that deposited as siliceous
450   gel, which was converted to chert during diagenesis (Ledevin, 2019). The cyclical repeat of this process resulted in the formation of bedded sedimentary carbonate (Fig. 8a).

Some EPT bedded sedimentary carbonates (except the Dresser bedded carbonates) show an average $\delta^{13}C$ value of $1.85 \pm 0.48$‰ (Fig. 11). These is consistent with other reports on Strelley Pool stromatolites (Lindsay et al., 2005; Flannery et al., 2018) and

within the range of modern seawater (Kroopnick, 1980; Tan, 1988), reflecting their formation in marine environments. At the same time, $\delta^{13}C$ values of the Dresser bedded carbonates are relatively depleted (-5.72 ±1.36 ‰ on average), in good accordance with $\delta^{13}C$ signatures of carbonatites (-4.99 ± 1.22 ‰ on average) (Fig.11), indicating hydrothermal admixture of mantle-derived carbon. The occurrence of rippled volcanic clastic sediments atop (Fig. 6e) indicates a shallow water environment. The clusters of radiating calcite crystals at the base of each carbonate-chert layer (Figs. 6f, 8a), which were initially proposed to be gypsum or aragonite (Runnegar et al., 2001; Van Kranendonk et al., 2008; Otálora et al., 2018), are likely indicative of evaporitic conditions. The $\delta^{13}C$ values and field relationships imply that the Dresser bedded carbonates perhaps formed in a terrestrial hydrothermal pond with intermittent inputs, akin to recently identified hot spring deposits (Djokic et al., 2017, 2021). Hence, bedded sedimentary carbonates formed across a spectrum of environments, ranging from shallow marine to terrestrial settings.

### 5.1.3 Stromatolites formed through microbial activity

Stromatolites, first described by Kalkowsky (1908), are defined as laminated benthic microbial deposits (Hofmann, 1973; Buick et al., 1981; Riding, 1999; Flügel, 2010). Although the biogenicity of early Archean stromatolites is commonly controversial, that of stromatolites from the Dresser Formation and the SPF has been widely accepted (Lambert et al. 1978; Van Kranendonk 2006, 2007; Allwood et al. 2006a, 2007, 2009; Marshall et al. 2007; Wacey, 2010; Bontognali et al., 2012; Duda et al. 2016; Flannery et al. 2018; Mißbach et al., 2021; Weimann et al., 2024). Carbonates associated with SPF stromatolites are thought to be related to microbial processes (Van Kranendonk 2007, 2011; Lepot, 2020).

Stromatolites typically form through biologically induced or controlled mineralization within microbial mats or biofilms, commonly related to physicochemical gradients and/or organic substances providing nucleation sites for mineral precipitation (Reitner et al., 2000). In any case, extracellular polymeric substances (EPS) secreted by microorganisms play a key-role in mineralization (Decho, 2011; see in Fig. 10). Certain functional groups of organic substances in the EPS (e.g. Asp- and Glu-rich macromolecules) efficiently bind and sequester divalent cations such as $Ca^{2+}$ and $Mg^{2+}$, thereby inhibiting their combination with carbonate anions and subsequent precipitation (Reitner et al. 1995a, b, c). This process is somewhat similar to organo-mineralization, which involves a mineralization of organic matrices and compounds decoupled from the source organisms or of abiotic origin (Trichet and Défarge, 1995; Défarge et al., 2009; Défarge, 2011). In case of EPS-controlled biomineralization, carbonate nucleation and growth are extracellular processes, which are triggered by the metabolic activity of microorganisms and related changes in the immediate environment (Heim, 2011).

EPS-controlled biomineralization might have played a role in case of the SPF stromatolites, as supported by $\delta^{13}C$ signatures of carbonates. More specifically, $\delta^{13}C$ values of carbonates from SPF stromatolites (3.08 ± 0.30 ‰ on average) are higher than those of the interstitial carbonates (0.22 ± 0.98 ‰ on average) and the sedimentary carbonates (1.85 ± 0.48‰ on average). This difference is well in line with a sequestration of $^{12}C$ by photoautotrophic microorganisms in the microbial mats, resulting in an enrichment of $^{13}C$ in the environment and, consequently, in the carbonate (e.g., Arp et al., 2011). Additionally, the positive $\delta^{13}C$ values of the SPF stromatolites are distinctive to those of rhodochrosite from the Fig Tree Group and of carbonate

inclusions in black barites of the Dresser Formation (-16.03 ± 4.86 ‰ and -12.56 ± 4.10 ‰ on average, respectively; Fig. 11), which are assumed to precipitate from microbial biomineralization and hydrothermal carbon. Flannery et al. (2018) reported a substantial $\delta^{13}C_{org}$ fractionation in SPF stromatolites and fan-like carbonates (similar to the materials investigated herein),
490 ranging from -29 to -45 ‰. It is documented to be compelling evidence for the coexistence of autotrophic possibly anoxygenic photosynthesis or predominantly heterotrophic metabolisms alongside the Calvin-Benson-Bassham (CBB) cycle (Flannery et al., 2018). Anoxygenic phototrophs appear to be plausible candidate microorganisms, given that they likely appeared about 3.8–3.4 billion years ago (Awramik, 1992; Brasier et al., 2006; Moore et al., 2017; Lepot, 2020). Taken together, carbonates associated with SPF stromatolites precipitated in shallow marine environments, perhaps lagoon-like, relatively restricted basin
495 (see Fig.12).

## 5.2 Early Archean carbonate factories – implications

Depending on the formation mechanisms, the identified EPT carbonates can be assigned to three carbonate factories: (i) an oceanic crust factory, (ii) an organo-carbonate factory, and (iii) a microbial carbonate factory. The formation pathways and depositional environments are summarized in Table 2. The oceanic crust factory includes abiotically formed carbonates such
500 as Mn- or Sr-enriched calcite and ankerite that are associated with pillow basalts within the upper oceanic crust. Carbonates in this carbonate factory precipitated from $CO_2$-rich seawater-derived hydrothermal fluids characterized by a high alkalinity and high cation loads. The organo-carbonate factory is dominated by authigenic carbonates formed through taphonomy-controlled organo-mineralization (i.e. organomicrites). Importantly, and in contrast to the microbial carbonate factory, the involved organic matter can be of either biological or abiotic origin. For this reason, precipitates assigned to this carbonate
505 factory formed in various environments, ranging from shallow marine to terrestrial settings. The microbial carbonate factory is somewhat similar to the organo-carbonate factory, but specifically refers to EPS-controlled carbonate precipitation, that is, mineralization of biologically derived organic substances. However, as in case of the organo-carbonate factory, organomicrite is formed as a typical product. Since this carbonate factory is directly linked to biological activity, the assigned precipitates typically occur in the photic, relatively restricted, shallow marine environments like lagoons. Given that most of these
510 carbonates formed in shallow-water environments under anoxic conditions, anoxygenic phototrophs appear a plausible source of biological organic matter, but this remains to be tested in future studies.

**Table 2: Features of the three carbonate factories in the early Archean**

| Features | Oceanic crust factory | Organo-carbonate factory | Microbial carbonate factory |
|---|---|---|---|
| Primary lithology | Acicular crystal-fan calcite | Organomicrite, calcite or ankerite crystals of various size, on a chert matrix | Laminated dolomite layers cemented by chert |

| | | | |
|---|---|---|---|
| Secondary lithology | Sparite, blocky, massive calcite and ankerite | Anhedral dolomite crystals showing compaction and pressure dissolution | Several generations of dolomites, including prismatic dolomite cement |
| Organic Materials (OM) | Absent | Abundant | Abundant |
| Origins of OM | - | Abiotic to biogenic | Biogenic |
| Hydrothermal inputs | Dominant | Common | Rare |
| Main origins of carbonate | Inorganic precipitation from seawater or seawater-derived hydrothermal fluids | Taphonomy-controlled organo-mineralization | EPS-controlled microbial mineralization |
| Evaporite minerals | Absent | Common to rare | Common to rare |
| Silicon in fluid | Source/sink | Sink | Sink |
| Siliciclastic sediments | Absent | Common | Common |
| Depositional setting | Deeper marine within the upper ocean basaltic crust | Diverse, shallow ocean to terrestrial hydrothermal pond | Photic shallow marine slope/ platform |

In case of all three carbonate factories, hydrothermal fluids play a key role in the formation and preservation of carbonate precipitates. The precipitation of carbonates might for instance be directly driven by basalt-alteration, or rather indirectly by providing a nutrient source for EPS-forming microorganisms. Preservation of carbonates is commonly promoted by hydrothermally driven silicification in the environment or during early diagenesis, which is well known for carbonaceous materials in early Archean rocks (Glikson et al., 2008; Alleon et al., 2016; Duda et al., 2016, 2018; van Zuilen, 2019; Hickman-Lewis, 2019; Ledevin, 2019; Lepot, 2020). Our study shows that such processes are also critical for the preservation of very delicate features in carbonates, allowing for the identification of precipitates formed in the three carbonate factories.

## 5.3 Carbon sinks during the early Archean

The Earth's surface carbon cycle is largely determined by mantle-derived atmospheric $CO_2$ as the single carbon source and biologically-derived organic carbon burial and carbonate sedimentation as the two main carbon sinks (Gislason and Oelkers, 2014; Hoefs, 2018; Shields, 2019). The carbon isotope ratios of the source ($\delta^{13}C$ of mantle $CO_2$ = -5 ‰) and the carbon sinks ($\delta^{13}C$ of organic matter = -25 ‰, $\delta^{13}C$ of seawater carbonate = 0 ‰) have remained largely constant throughout Earth history

(Schidlowski, 1988). Following a simple carbon isotope mass balance equation (see Eq. 2), in which the carbon input to the surface reservoirs is balanced by these two sinks only, it follows that the fraction of organic carbon that is buried relative to the total carbon input ($f_{org}$) has remained constant since the early Archean, with a value of ca. 0.2 (Hayes et al., 1999). Since

530 the burial of organic carbon is directly linked to the flux of oxygen to the atmosphere (Campbell and Allen, 2008; Hayes and Waldbauer, 2006), a constant $f_{org}$ would imply that the carbon cycle alone cannot explain the rise of atmospheric oxygen at 2.4 Ga (Krissansen-Totton et al., 2015). Rather, processes affecting the oxygen sink would have to be invoked, such as e.g. a change from predominantly subaerial volcanism to submarine volcanism (Kump and Barley, 2007), mantle redox evolution (Kasting et al., 1993), or atmospheric hydrogen escape (Catling et al., 2001; Claire et al., 2006; Zahnle et al., 2013).

535 Alternatively, the classical carbon isotope mass balance equation requires refinement, since it does not take into account key carbonate sinks such as oceanic crust carbonatization (briefly OCC, Bjerrum and Canfield, 2004) and authigenic carbonate that precipitates inorganically in situ (Schrag et al., 2013).

In the early Archean, when continental crustal mass was much less than today (Taylor and McLennan, 1981; Arndt, 1999; Flament et al., 2008; Cawood et al., 2013; Korenaga, 2021) and thus terrestrial silicate weathering was minimal or even absent,

540 OCC would have been the dominant carbonate sink. The fraction of OCC of the total inorganic carbon sink ($\lambda$), was estimated by Bjerrum and Canfield (2004) to have evolved from 0.95 in the early Archean to 0.39 at the onset of the Phanerozoic. Taking this into account in an extended carbon isotope mass balance equation (Bjerrum and Canfield, 2004), it is shown that the fraction of organic carbon burial $f_{org}$ was likely much lower than today, with values closer to 0.1. Critically important in this extended mass balance is the carbon isotope ratio of the OCC, which was estimated by Bjerrum and Canfield (2004) based on

545 micritic siderites in deep-water BIF's ($\delta^{13}C$ of -5 to -3 ‰) and modern seafloor hydrothermal carbonate deposits ($\delta^{13}C$ of -2 to 0 ‰).

The carbon isotope ratios that we report here for the three carbonate factories can now be used to verify this carbon isotope mass balance calculation. Bjerrum and Canfield (2004) postulated that total inorganic carbon removal comprises two primary fluxes, sedimentary carbonate carbon (SCC) and OCC (Fig. 13). The OCC-mediated carbon removal is expressed as a fraction

550 ($\lambda$) of the total. Based on this, isotopic mass balance equations may be written as:

$$\delta^{13}C_{in} = \delta^{13}C_{org}f_{org} + \delta^{13}C_{IC}(1 - f_{org}) \qquad \text{(Eq.2)}$$

$$\delta^{13}C_{IC} = \delta^{13}C_{OCC}\lambda + \delta^{13}C_{SCC}(1 - \lambda) \qquad \text{(Eq.3)}$$

where $\delta^{13}C_{in}$ represents the isotopic ratio of carbon entering oceans; $\delta^{13}C_{IC}$, $\delta^{13}C_{OCC}$ and $\delta^{13}C_{SCC}$ respectively signify the isotopic ratios of total inorganic carbon precipitated as carbonate, carbonate in ocean crust and sediment; $f_{org}$ denotes the

555 fraction of organic carbon ($\delta^{13}C_{org}$) removed from total oceanic carbon. Then Eq. 2 can be rewritten in conjunction with Eq. 3 as:

$$\delta^{13}C_{in} = \delta^{13}C_{SCC} + f_{org}\left(\delta^{13}C_{org} - \delta^{13}C_{SCC}\right) + \lambda(1 - f_{org})(\delta^{13}C_{OCC} - \delta^{13}C_{SCC}) \qquad \text{(Eq.4)}$$

Given $\Delta_S = \delta^{13}C_{OCC} - \delta^{13}C_{SCC}$ and $\Delta_b = \delta^{13}C_{org} - \delta^{13}C_{SCC}$, then the following isotopic mass balance is obtained:

$$\delta^{13}C_{in} = \delta^{13}C_{SCC} + f_{org}\Delta_b + \lambda(1 - f_{org})\Delta_S \qquad \text{(Eq.5)}$$

where $\Delta_S$ and $\Delta_b$ represent the isotopic differences between the inorganic carbon removed by OCC and SCC, organic carbon and SCC, respectively.
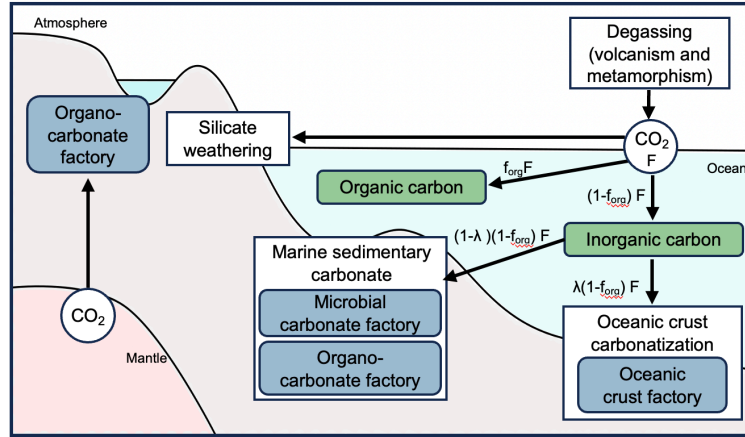
**Figure 13: Simplified carbon sinks in the early Archean. Carbon entering the ocean (F) was partitioned: a fraction ($f_{org}$) converted to organic carbon, while the remainder (1-$f_{org}$) became inorganic carbon as carbonates. Carbonate carbon was further divided, with a fraction ($\lambda$) sequestered in the oceanic crust factory and the rest processed in microbial and organo-carbonate factories. The green boxes represent two carbon sinks in ocean; blue boxes depict three carbonate factories; solid arrows indicate carbon flux (adapted from Mills et al., 2014).**

By utilizing the $\delta^{13}C$ range of carbonate in the oceanic crust factory (-2.37 to 0.99 ‰) as a reference for OCC, and those of marine sedimentary carbonate from the organo-carbonate (1.10 to 2.55 ‰) and microbial carbonate factories (2.46 to 3.38 ‰) combined for SCC (1.10 to 3.38 ‰), we estimate a $f_{org}$ range of 0.10-0.20 (Table 3), consistent with Bjerrum and Canfield (2004). Assuming an extreme case where OCC contributes only 50 % (i.e. $\lambda$=0.5) of the total inorganic carbon sink, $f_{org}$ remains below 0.23, a scenario deemed unlikely based on field observations. The observed $f_{org}$ range closely matches previous estimates for both the early Archean (Krissansen-Totton et al., 2015) and modern times (Hayes et al., 1999; Berner, 2004), highlighting the prevalence of carbonates, particularly those in the oceanic crust factory, as primary carbon sinks during early Earth's history.

**Table 3: Parameters used in calculating carbon isotopic mass balance**

| $\delta^{13}C_{in}$ [a] | $\delta^{13}C_{org}$ [a] | $\delta^{13}C_{SCC}$ | $\delta^{13}C_{OCC}$ [b] | $\Delta_S$ | $\Delta_b$ | $\lambda$ | $f_{org}$ |
|---|---|---|---|---|---|---|---|
| -5.0 | -30.0 | 0.0 [a] | -2.37 | -2.4 | -30.0 | 0.95 [a] | 0.099 |
| -5.0 | -30.0 | 0.0 [a] | 0.99 | 1.0 | -30.0 | 0.95 [a] | 0.192 |
| -5.0 | -30.0 | 1.1 [c] | -2.37 | -3.5 | -31.1 | 0.95 [a] | 0.101 |
| -5.0 | -30.0 | 1.1 [c] | 0.99 | -0.1 | -31.1 | 0.95 [a] | 0.193 |
| -5.0 | -30.0 | 3.4 [d] | -2.37 | -5.8 | -33.4 | 0.95 [a] | 0.105 |

| | | | | | | | |
|---|---|---|---|---|---|---|---|
| -5.0 | -30.0 | 3.4 [d] | 0.99 | -2.4 | -33.4 | 0.95 [a] | 0.196 |
| -5.0 | -30.0 | 3.4 [d] | -2.37 | -5.8 | -33.4 | 0.70 | 0.148 |
| -5.0 | -30.0 | 3.4 [d] | 0.99 | -2.4 | -33.4 | 0.70 | 0.212 |
| -5.0 | -30.0 | 3.4 [d] | -2.37 | -5.8 | -33.4 | 0.50 | 0.180 |
| -5.0 | -30.0 | 3.4 [d] | 0.99 | -2.4 | -33.4 | 0.50 | 0.223 |

**Note: superscript a, b, c, and d respectively indicate data from Bjerrum and Canfield (2004), the max/min $\delta^{13}C$ values of carbonates in the oceanic crust factory, the min carbonate $\delta^{13}C$ in the organo-carbonate factory, and the max carbonate $\delta^{13}C$ in the microbial carbonate factory.**

The prevalence of carbonatized greenstones during the early Archean era underscores the significance of oceanic crust factory and OCC (Kitajima et al., 2001; Nakamura and Kato, 2002, 2004; Anhaeusser, 2014; Kasting, 2019; Nutman et al., 2019a). Estimates of $CO_2$ fluxes from ocean to crust during this period, based on carbonate abundance, exceed $3.8 \times 10^{13}$ mol/yr in the early and $1.5 \times 10^{14}$ mol/yr in the middle Archean (Nakamura and Kato, 2004; Shibuya et al., 2012), markedly higher (1-2 orders) than modern fluxes ($1.5–2.4 \times 10^{12}$ mol/yr; Alt and Teagle, 1999). Importantly, prior studies overlooked interstitial carbonates due to quantification difficulties. Our preliminary volumetric assessments suggest a higher proportion of interstitial carbonates than carbonate minerals in basalts (Figs. 3a and 5b), implying a more pivotal role for oceanic crust factory and SCC in shaping the early Archean global carbon cycle than previously thought (Nakamura and Kato, 2004; Shibuya et al., 2012; Coogan and Gillis, 2013).

To assess its significance in the carbon cycle, we estimated carbon flux to the early Archean oceanic crust, focusing on pillow basalts that retain primary interstitial calcite due to uncertainty in altered samples' post-depositional timing. The carbon flux is quantitatively approximated by the product of two key factors: firstly, the carbon incorporated into interstitial calcite, arising from the interaction of seawater, $CO_2$ and basaltic oceanic crust during OCC (see Eq.1), and secondly, the rate of production of altered oceanic crust. It can be written as:

$$F_C = F_{Ca} = R_{cc} \times C_{Ca} \times L_{Ca} / M_{Ca} \qquad\qquad (Eq.6)$$

where $F_C$ is the carbon flux into the oceanic crust factory (mol/yr), $F_{Ca}$ is the released calcium flux during OCC (mol/yr), $C_{Ca}$ is the Ca concentration of the oceanic crust, $L_{Ca}$ is the Ca loss during SCC (%), $M_{Ca}$ is the molar mass of Ca (g/mol), and $R_{cc}$ is the production rate of the carbonatized oceanic crust (g/yr). The $R_{cc}$ can be further estimated by Eq.7:

$$R_{cc} = sp \times D \times \rho \qquad\qquad (Eq.7)$$

where $sp$ is the spreading rate of oceanic crust ($cm^2$/yr), D is the depth of carbonatized zone (cm), and $\rho$ is the density of oceanic crust (g/$cm^3$).

600  To enable a comparison with Nakamura and Kato's (2004) results, we used specific parameters: D and *sp* (500 m and 1.8 ×
$10^{11}$ cm²/yr, respectively; Nakamura and Kato, 2004), ρ (3.0 g/cm³, akin to modern basalt; Karato, 1983), $C_{Ca}$ (2.61 wt%,
matching Primitive Mantle; Palme and O'Neil, 2014), $L_{Ca}$ (22.57 %, see Appendix C), and $M_{Ca}$ (40 g/mol). Our calculation
revealed a carbon flux of 3.8 × $10^{12}$ mol/yr into the oceanic crust factory, one order of magnitude lower than Nakamura and
Kato's oceanic crust flux (3.8 × $10^{13}$ mol/yr). This difference contrasts with volumetric estimates from thin section analysis,
605  suggesting an issue. Accuracy of μXRF-derived $L_{Ca}$ values, limited by reference materials, may affect representativeness.
However, even assuming complete Ca loss from PM during alteration ($L_{Ca}$ of 100%), our oceanic crust factory flux estimate
remains lower (1.8 × $10^{13}$ mol/yr). This discrepancy hints at an overestimation of average carbon content (1.4 × $10^{-3}$ mol/g)
in Nakamura and Kato's study, warranting a reassessment of assumptions and methodologies.

Despite uncertainties, the early Archean oceanic crust factory likely served as a significant carbon sink. Integrating modern
610  and Archean data, seafloor weathering carbon flux at 3.46 Ga was estimated at 7.6-65 × $10^{12}$ mol/yr (Krissansen-Totton et al.,
2018). The same calculation using our data yields a flux range of 0.76 – 6.5 × $10^{12}$ mol/yr. This range is similar to estimates
assuming Archean continental weathering but below those which do no (Krissansen-Totton et al., 2018). Remarkably, modern
oceanic crust seems to lack a carbonate factory as observed in the early Archean; carbonate minerals occur primarily in veins,
vesicles, and breccias, with greater abundance in older crusts (Gillis et al., 2001; Heft et al., 2008; Coogan and Gillis, 2013).
615  This carbonate factory's carbon flux approximates that in modern oceanic crusts (1.0-2.4 × $10^{12}$ mol/yr; Alt and Teagle, 1999;
Rausch, 2012). This underscores the pivotal role of the oceanic crust factory as a major carbon sink on the early Earth's surface,
while simultaneously elucidating the previously underestimated contributions of OCC to the carbon cycle and its potent
capacity as a climate-modulating buffer during that epoch.

In summary, constraining carbon flux dynamics in the early Archean is challenging due to uncertainties in quantifying
620  carbonate reservoirs. Despite limitations, estimates based on carbon isotope mass balancing across carbonate factories and
carbon flux in oceanic crust suggest they were significant carbon sinks. These factories were fundamental to the carbon cycle,
acting as buffers that modulated early Earth's climate.

**6 Conclusion**

Paleoarchean rocks in the Pilbara Craton (Western Australia) contain carbonates of various origin. Three carbonate factories
625  are recognized: (i) an oceanic crust factory, (ii) an organo-carbonate factory, and (iii) a microbial carbonate factory. The
oceanic crust factory is characterized by carbonates associated with pillowed basalts, which precipitated abiotically on and
within basaltic oceanic crust from $CO_2$-enriched seawater and seawater-derived alkaline hydrothermal fluids. The organo-
carbonate factory encompasses carbonate that formed via taphonomy-controlled organo-mineralization linked to organic
macromolecules (either biotic or abiotic). The microbial carbonate factory includes carbonates formed through mineralization
630  controlled by microbial extracellular polymeric substances (EPS). In case of all three carbonates factories, hydrothermal fluids
seem to play also an important role in the formation and preservation of mineral precipitates. Carbon isotope mass balances
reveal a $f_{org}$ range of 0.10-0.20, close to what is known from modern Earth. Likewise, the estimated carbon flux into the oceanic

crust factory ($0.76-6.5 \times 10^{12}$ mol/yr) is similar to that by oceanic crust carbonatization in the modern ocean. Hence, oceanic-crust related carbon cycling during the early Archean has been somewhat similar to today. Our study underscores the value of Paleoarchean carbonates as geobiological archives and emphasizes their importance as major carbon sinks on the early Earth, highlighting their potential role in modulating the carbon cycle and, consequently, shaping climate variability.

*Data availability.* The data are presented in the manuscript; and can be requested from the corresponding author.

*Author contribution.* Xiang, Reitner and Duda designed the framework and methodology of this study. Reitner and van Zuilen contributed to the fieldwork, sample and data collections. Pack was involved in data interpretation. Xiang is responsible for data collection, analysis and interpretation, and drafting the manuscript. All co-authors have been involved in revising the content of the manuscript, and approved the final manuscript for submission.

*Competing interests*. The authors declare that they have no conflict of interest.

*Acknowledgements.* We thank A. Hackmann and W. Dröse for sample preparation, B. Schmidt, J. Schönig for their help with Raman spectroscopy and µXRF, A. Kronz for carrying out EPMA mappings, and T. Di Rocco, D. Kohl and T. Wasselin for stable isotope measurements, all geoscience faculty of University of Göttingen. M. van Kranendonk (Curtain University Perth, Western Australia) as well as F. Myers and G. Myers acknowledged for their assistance in the field and providing rock material. A. Hickman (Geological Survey of Western Australia) and A. Hofmann (University of Johannesburg, South Africa) thanked for providing information of the Pilbara Craton and the Barberton Greenstone Belt, respectively. The core library of the Geological Survey of Western Australia, is acknowledged for permission to sample drill core materials from the Pilbara region (approval for P954, 1014, 1091). This study was financially supported by the China Council Scholarship (CSC), the German Research Foundation (DFG) priority program (SPP)1833 "Building a Habitable Earth" (RE 665/42-2; DU 1450/3-1, DU 1450/3-2; TH 713/13-2), the Göttingen Academy of Sciences and Humanities in Lower Saxony, and Leshan Normal University Scientific Research Start-up Project for Introducing High-level Talents (RC2024007).

# References

Addadi, L., Weiner, S.: Interactions between acidic proteins and crystals: stereochemical requirements in biomineralization, Proceedings of the National Academy of Sciences, 82, 4110-4114, 1985.

Addadi, L., Raz, S., and Weiner, S.: Taking advantage of disorder: amorphous calcium carbonate and its roles in biomineralization, Advanced Materials, 15, 959–970, https://doi.org/10.1002/adma.200300381, 2003.

Alleon, J., Bernard, S., Le Guillou, C., Daval, D., Skouri-Panet, F., Pont, S., Delbes, L., and Robert, F.: Early entombment within silica minimizes the molecular degradation of microorganisms during advanced diagenesis, Chemical Geology, 437, 98–108, 2016.

Allwood, A. C., Walter, M. R., Kamber, B. S., Marshall, C. P., and Burch, I. W.: Stromatolite reef from the Early Archaean era of Australia, Nature, 441, 714–718, 2006a.

Allwood, A. C., Walter, M. R. , & Marshall, C. P.: Raman spectroscopy reveals thermal palaeoenvironments of c.3.5 billion-year-old organic matter. Vibrational Spectroscopy, 41, 190-197, 2006b.

Allwood, A. C., Walter, M. R., Burch, I. W., and Kamber, B. S.: 3.43 billion-year-old stromatolite reef from the Pilbara Craton of Western Australia: ecosystem-scale insights to early life on Earth, Precambrian Research, 158, 198–227, 2007.

Allwood, A. C., Grotzinger, J. P., Knoll, A. H., Burch, I. W., Anderson, M. S., Coleman, M. L., and Kanik, I.: Controls on development and diversity of Early Archean stromatolites, Proceedings of the National Academy of Sciences, 106, 9548–9555, 2009.

Allwood, A. C., Kamber, B. S., Walter, M. R., Burch, I. W., and Kanik, I.: Trace elements record depositional history of an Early Archean stromatolitic carbonate platform, Chemical Geology, 270, 148–163, 2010.

Allwood, A. C., Rosing, M. T., Flannery, D. T., Hurowitz, J. A., and Heirwegh, C. M.: Reassessing evidence of life in 3,700-million-year-old rocks of Greenland, Nature, 563, 241–244, 2018.

Alt, J. C. and Teagle, D. A.: The uptake of carbon during alteration of ocean crust, Geochimica et Cosmochimica Acta, 63, 1527–1535, 1999.

Altermann, W., Böhmer, C., Gitter, F., Heimann, F., Heller, I., Läuchli, B., and Putz, C.: Defining Biominerals and Organominerals: Direct And Indirect Indicators Of Life. Perry et al., Sedimentary Geology, 201,157-179, Sedimentary Geology, 213, 150–151, https://doi.org/10.1016/j.sedgeo.2008.04.001, 2009.

Andersen, T. and Taylor, P. N.: Pb isotope geochemistry of the Fen carbonatite complex, SE Norway: Age and petrogenetic implications, Geochimica et Cosmochimica Acta, 52, 209–215, https://doi.org/10.1016/0016-7037(88)90069-5, 1988.

Anhaeusser, C. R.: Archaean greenstone belts and associated granitic rocks–a review, Journal of African Earth Sciences, 100, 684–732, 2014.

Arndt, N.: Why was flood volcanism on submerged continental platforms so common in the Precambrian?, Precambrian Research, 97, 155–164, 1999.

Arp, G., Reimer, A., and Reitner, J.: Calcification in cyanobacterial biofilms of alkaline salt lakes, European Journal of Phycology, 34, 393—403, 1999.

Arp, G., Reimer, A., and Reitner, J.: Photosynthesis-induced biofilm calcification and calcium concentrations in Phanerozoic oceans, Science, 292, 1701–1704, 2001.

Arp, G., Reimer, A., and Reitner, J.: Microbialite formation in seawater of increased alkalinity, Satonda Crater Lake, Indonesia, Journal of Sedimentary Research, 73, 105—-127, 2003.

Arp, G., Helms, G., Karlinska, K., Schumann, G., Reimer, A., Reitner, J., and Trichet, J.: Photosynthesis versus Exopolymer Degradation in the Formation of Microbialites on the Atoll of Kiritimati, Republic of Kiribati, Central Pacific. Geomicrobiology Journal, 29(1), 29–65. https://doi.org/10.1080/01490451.2010.521436, 2011.

695    Awramik, S. M.: The oldest records of photosynthesis, Photosynthesis research, 33, 75–89, https://doi.org/10.1007/BF00039172, 1992.

Bach, W., Alt, J. C., Niu, Y., Humphris, S. E., Erzinger, J., and Dick, H. J.: The geochemical consequences of late-stage low-grade alteration of lower ocean crust at the SW Indian Ridge: Results from ODP Hole 735B (Leg 176), Geochimica et Cosmochimica Acta, 65, 3267–3287, 2001.

700    Bach, W., Peucker-Ehrenbrink, B., Hart, S. R., and Blusztajn, J. S.: Geochemistry of hydrothermally altered oceanic crust: DSDP/ODP Hole 504B–Implications for seawater-crust exchange budgets and Sr-and Pb-isotopic evolution of the mantle, Geochemistry, Geophysics, Geosystems, 4, 2003.

Bach, W., Rosner, M., Jöns, N., Rausch, S., Robinson, L. F., Paulick, H., and Erzinger, J.: Carbonate veins trace seawater circulation during exhumation and uplift of mantle rock: Results from ODP Leg 209, Earth and Planetary Science Letters, 311,

705    242–252, 2011.

Berner, R. A.: The Phanerozoic Carbon Cycle: $CO_2$ and $O_2$, Oxford University Press, https://doi.org/10.1093/oso/9780195173338.001.0001, 2004.

Bontognali, T. R., Sessions, A. L., Allwood, A. C., Fischer, W. W., Grotzinger, J. P., Summons, R. E., and Eiler, J. M.: Sulfur isotopes of organic matter preserved in 3.45-billion-year-old stromatolites reveal microbial metabolism, Proceedings of the

710    National Academy of Sciences, 109, 15 146–15 151, 2012.

Bower, D., Steele, A., Fries, M., Green, O., and Lindsay, J.: Raman imaging spectroscopy of a putative microfossil from the 3.46 Ga Apex chert: Insights from quartz grain orientation, Astrobiology, 16, 169–180, 2016.

Brasier, M. D., Green, O. R., Jephcoat, A. P., Kleppe, A. K., Van Kranendonk, M. J., Lindsay, J. F., Steele, A., and Grassineau, N. V.: Questioning the evidence for Earth's oldest fossils, Nature, 416, 76–81, 2002.

715    Brasier, M., Green, O., Lindsay, J., and Steele, A.: Earth's Oldest ( 3.5 Ga) Fossils and theEarly Eden Hypothesis': Questioning the Evidence, Origins of Life and Evolution of the Biosphere, 34, 257–269, 2004.

Brasier, M. D., Green, O. R., Lindsay, J. F., McLoughlin, N., Steele, A., and Stoakes, C.: Critical testing of Earth's oldest putative fossil assemblage from the 3.5 Ga Apex chert, Chinaman Creek, Western Australia, Precambrian Research, 140, 55–102, 2005.

720    Brasier, M., McLoughlin, N., Green, O., and Wacey, D.: A fresh look at the fossil evidence for early Archaean cellular life, Philosophical Transactions of the Royal Society B: Biological Sciences, 361, 887–902, 2006.

Brasier, M. D., Antcliffe, J., Saunders, M., and Wacey, D.: Changing the picture of Earth's earliest fossils (3.5–1.9 Ga) with new approaches and new discoveries, Proceedings of the National Academy of Sciences, 112, 4859–4864, 2015.

Buick, R., Dunlop, J., and Groves, D.: Stromatolite recognition in ancient rocks: an appraisal of irregularly laminated structures

725    in an Early Archaean chert-barite unit from North Pole, Western Australia, Alcheringa, 5, 161–181, https://doi.org/10.1080/03115518108566999, 1981.

Byerly, G. R., Lowe, D. R., Wooden, J. L., and Xie, X.: An Archean impact layer from the Pilbara and Kaapvaal cratons, Science, 297, 1325–1327, 2002.

Campbell, I., Allen, C. Formation of supercontinents linked to increases in atmospheric oxygen. *Nature Geoscience* **1**, 554–558, https://doi.org/10.1038/ngeo259, 2008.

Canfield, D. E.: Carbon cycle evolution before and after the Great Oxidation of the atmosphere, American Journal of Science, 321, 297–331, https://doi.org/10.2475/03.2021.01, 2021.

Catling, D. C. and Zahnle, K. J.: The Archean atmosphere, Science advances, 6, eaax1420, 2020.

Catling, D. C., Zahnle, K. J., and McKay, C. P.: Biogenic Methane, Hydrogen Escape, and the Irreversible Oxidation of Early Earth, Science, 293, 839–843, https://doi.org/10.1126/science.1061976, 2001.

Cawood, P. A., Hawkesworth, C., and Dhuime, B.: The continental record and the generation of continental crust, Geological Society of America Bulletin, 125, 14–32, 2013.

Ciais, P., Chris, S., Govindasamy, B., Bopp, L., Brovkin, V., Canadell, J., Chhabra, A., Defries, R., Galloway, J., and Heimann, M.: Carbon and other biogeochemical cycles, in: Climate Change 2013: The Physical Science Basis. Contribution of Working Group I to the Fifth Assessment Report of the Intergovernmental Panel on Climate Change, edited by Stocker, T.F., D. Qin, G.-K. Plattner, M. Tignor, S.K. Allen, J. Boschung, A. Nauels, Y. Xia, V. Bex and P.M. Midgley, Cambridge University Press, pp. 465-570, 2013.

Claire, M., Catling, D., and Zahnle, K.: Biogeochemical modelling of the rise in atmospheric oxygen, Geobiology, 4, 239 –269, https://doi.org/10.1111/j.1472-4669.2006.00084.x, 2006.

Coogan, L. A. and Gillis, K. M.: Evidence that low-temperature oceanic hydrothermal systems play an important role in the silicate-carbonate weathering cycle and long-term climate regulation, Geochemistry, Geophysics, Geosystems, 14, 1771–1786, 2013.

Coplen, T. B.: Normalization of oxygen and hydrogen isotope data, Chemical Geology: Isotope Geoscience section, 72, 293–297, https://doi.org/10.1016/0168-9622(88)90042-5, 1988.

Decho, A. W.: Extracellular polymeric substances (EPS), in: Encyclopedia of Geobiology, edited by Reitner, J. and Thiel, V., pp. 359–361, Springer, Berlin, 2011.

Défarge, C.: Organomineralization, in: Encyclopedia of geobiology, edited by Reitner, J. and Thiel, V., pp. 697-701, Springer, Berlin, 2011.

Défarge, C. and Trichet, J.: From biominerals to 'organominerals': The example of the modern lacustrine calcareous stromatolites from Polynesian atolls, in: Bulletin de l'Institut Océanographique de Monaco, n∘ spéc. 14, edited by Allemand, D. and Cuif, J., vol. 2, pp. 265—271, Proc. 7th Int. Symp. Biomineralization, 1995.

Défarge, C., Gautret, P., Reitner, J., and Trichet, J.: Defining Organominerals: Comment On 'defining Biominerals And Organominerals: Direct And Indirect Indicators Of Life' By Perry et al.(2007, Sedimentary Geology, 201,157-179), Sedimentary Geology, 213, 152–155, https://doi.org/10.1016/J.SEDGEO.2008.04.002, 2009.

Degens, E. T., Wong, H.-K., Kempe, S., and Kurtman, F.: A geological study of Lake Van, eastern Turkey, Geologische Rundschau, 73, 701–734, https://doi.org/10.1007/BF01824978, 1984.

Delarue, F., Robert, F., Derenne, S., Tartèse, R., Jauvion, C., Bernard, S., Pont, S., Gonzalez-Cano, A., Duhamel, R., and Sugitani, K.: Out of rock: A new look at the morphological and geochemical preservation of microfossils from the 3.46 Gyr-old Strelley Pool Formation, Precambrian Research, 336, 105 472, 2020.

765 Djokic, T., Van Kranendonk, M. J., Campbell, K. A., Walter, M. R., and Ward, C. R.: Earliest signs of life on land preserved in ca. 3.5 Ga hot spring deposits, Nature communications, 8, 15 263, 2017.

Djokic, T., Van Kranendonk, M. J., Campbell, K. A., Havig, J. R., Walter, M. R., and Guido, D. M.: A reconstructed subaerial hot spring field in the 3.5 billion-year-old Dresser Formation, North Pole Dome, Pilbara Craton, Western Australia, Astrobiology, 21, 1–38, 2021.

770 Duda, J.-P., Van Kranendonk, M. J., Thiel, V., Ionescu, D., Strauss, H., Schäfer, N., and Reitner, J.: A rare glimpse of Paleoarchean life: Geobiology of an exceptionally preserved microbial mat facies from the 3.4 Ga Strelley Pool Formation, Western Australia, PLoS One, 11, e0147 629, 2016.

Duda, J.-P., Thiel, V., Bauersachs, T., Mißbach, H., Reinhardt, M., Schäfer, N., Van Kranendonk, M. J., and Reitner, J.: Ideas and perspectives: hydrothermally driven redistribution and sequestration of early Archaean biomass–the "hydrothermal pump hypothesis", Biogeosciences, 15, 1535–1548, 2018.

775 Escoffier, N., Perolo, P., Lambert, T., Rüegg, J., Odermatt, D., Adatte, T., Vennemann, T., and Perga, M.-E.: Whiting Events in a Large Peri-Alpine Lake: Evidence of a Catchment-Scale Process, Journal of Geophysical Research: Biogeosciences, 127, e2022JG006 823, 2022.

Flament, N., Coltice, N., and Rey, P. F.: A case for late-Archaean continental emergence from thermal evolution models and hypsometry, Earth and Planetary Science Letters, 275, 326–336, 2008.

780 Flannery, D. T., Allwood, A. C., Summons, R. E., Williford, K. H., Abbey, W., Matys, E. D., and Ferralis, N.: Spatially-resolved isotopic study of carbon trapped in 3.43 Ga Strelley Pool Formation stromatolites, Geochimica et Cosmochimica Acta, 223, 21–35, 2018.

Flügel, E.: Microfacies of carbonate rocks: analysis, interpretation and application, vol. 976, Springer, 2nd., 2010.

785 French, K. L., Hallmann, C., Hope, J. M., Schoon, P. L., Zumberge, J. A., Hoshino, Y., Peters, C. A., George, S. C., Love, G. D., Brocks, J. J., et al.: Reappraisal of hydrocarbon biomarkers in Archean rocks, Proceedings of the National Academy of Sciences, 112, 5915–5920, https://doi.org/10.1073/pnas.1419563112, 2015.

Galeczka, I., Wolff-Boenisch, D., and Gislason, S.: Experimental studies of basalt-$H_2O$-$CO_2$ interaction with a high pressure column flow reactor: the mobility of metals, Energy Procedia, 37, 5823–5833, https://doi.org/10.1016/j.egypro.2013.06.505, 790 2013a.

Galeczka, I., Wolff-Boenisch, D., Jonsson, T., Sigfusson, B., Stefansson, A., and Gislason, S.: A novel high pressure column flow reactor for experimental studies of $CO_2$ mineral storage, Applied Geochemistry, 30, 91–104, https://doi.org/10.1016/j.apgeochem.2012.08.010, 2013b.

Galeczka, I., Wolff-Boenisch, D., Oelkers, E. H., and Gislason, S. R.: An experimental study of basaltic glass–$H_2O$–$CO_2$ interaction at 22 and 50 °C: Implications for subsurface storage of $CO_2$, Geochimica et Cosmochimica Acta, 126, 123–145, https://doi.org/10.1016/j.gca.2013.10.044, 2014.

Gardiner, N. J., Wacey, D., Kirkland, C. L., Johnson, T. E., and Jeon, H.: Zircon U–Pb, Lu–Hf and O isotopes from the 3414 Ma Strelley Pool Formation, East Pilbara Terrane, and the Palaeoarchaean emergence of a cryptic cratonic core, Precambrian Research, 321, 64–84, https://doi.org/10.1016/j.precamres.2018.11.023, 2019.

Gautret, P. and Trichet, J.: Automicrites in modern cyanobacterial stromatolitic deposits of Rangiroa, Tuamotu Archipelago, French Polynesia: Biochemical parameters underlaying their formation, Sedimentary Geology, 178, 55–73, https://doi.org/10.1016/j.sedgeo.2005.03.012, 2005.

Geological Survey of Western Australia, cartographer, Western Australia. Department of Mines and Petroleum, and Exploration Incentive Scheme (W.A.): 1:100 000 GIS Pilbara 2013 update / Geological Survey of Western Australia, 2013.

Gillis, K. M., Muehlenbachs, K., Stewart, M., Gleeson, T., and Karson, J.: Fluid flow patterns in fast spreading East Pacific Rise crust exposed at Hess Deep, Journal of Geophysical Research: Solid Earth, 106, 26 311–26 329, https://doi.org/10.1029/2000JB000038, 2001.

Gislason, S. R. and Oelkers, E. H.: Carbon storage in basalt, Science, 344, 373–374, https://doi.org/10.1126/science.1250828, 2014.

Glikson, M., Duck, L. J., Golding, S. D., Hofmann, A., Bolhar, R., Webb, R., Baiano, J. C., and Sly, L. I.: Microbial re- mains in some earliest Earth rocks: comparison with a potential modern analogue, Precambrian Research, 164, 187–200, https://doi.org/10.1016/j.precamres.2008.05.002, 2008.

Gudbrandsson, S., Wolff-Boenisch, D., Gislason, S. R., and Oelkers, E. H.: An experimental study of crystalline basalt dissolution from $2 \leqslant pH \leqslant 11$ and temperatures from 5 to 75 C, Geochimica et Cosmochimica Acta, 75, 5496–5509, https://doi.org/10.1016/j.gca.2011.06.035, 2011.

Gysi, A. P. and Stefánsson, A.: $CO_2$–water–basalt interaction. Numerical simulation of low temperature $CO_2$ sequestration into basalts, Geochimica et Cosmochimica Acta, 75, 4728–4751, https://doi.org/10.1016/j.gca.2011.05.037, 2011.

Hayes, J. M. and Waldbauer, J. R.: The carbon cycle and associated redox processes through time, Philosophical Transactions of the Royal Society B: Biological Sciences, 361, 931–950, https://doi.org/10.1098/rstb.2006.1840, 2006.

Hayes, J. M., Strauss, H., and Kaufman, A. J.: The abundance of $^{13}C$ in marine organic matter and isotopic fractionation in the global biogeochemical cycle of carbon during the past 800 Ma, Chemical Geology, 161, 103–125, https://doi.org/https://doi.org/10.1016/S0009- 2541(99)00083-2, 1999.

Heft, K. L., Gillis, K. M., Pollock, M. A., Karson, J. A., and Klein, E. M.: Role of upwelling hydrothermal fluids in the development of alteration patterns at fast spreading ridges: Evidence from the sheeted dike complex at Pito Deep, Geochemistry, Geophysics, Geosystems, 9, https://doi.org/10.1029/2007GC001926, 2008.

Heim, C.: Microbial biomineralization, in: Encyclopedia of Geobiology, edited by Reitner, J. and Thiel, V., pp. 586–591, Springer, Berlin, 2011.

Heinrichs, T.: Lithostratigraphische Untersuchungen in der Fig Tree Gruppe des Barberton Greenstone Belt zwischen Umsoli und Lomati (Südafrika), Göttinger Arbeiten zur Geologie und Paläontologie, 22, 1-118, 1980

830 Hickman, A. H. and Van Kranendonk, M.: A Billion Years of Earth History: A Geological Transect Through the Pilbara Craton and the Mount Bruce Supergroup-a Field Guide to Accompany 34th IGC Excursion WA-2, Geological Survey of Western Australia, Record 2012/10, 2012a.

Hickman, A. H. and Van Kranendonk, M. J.: Early Earth evolution: evidence from the 3.5–1.8 Ga geological history of the Pilbara region of Western Australia, Episodes Journal of International Geoscience, 35, 283–297,

835 https://doi.org/10.18814/epiiugs/2012/v35i1/028, 2012b.

Hickman, A., Van Kranendonk, M., and Grey, K.: State Geoheritage Reserve R50149 (Trendall Reserve), North Pole, Pilbara Craton, Western Australia — geology and evidence for early Archean life. Geological Survey of Western Australia Record 2011/10, 2011.

Hickman-Lewis, K., Westall, F., and Cavalazzi, B.: Trace of early life in the Barberton greenstone belt, in: Earth's Oldest

840 Rocks, edited by Van Kranendonk, M., Bennett, V., and Hoffmann, E., pp. 1029–1058, Elsevier, https://hal.science/hal-03041208, 2019.

Hoefs, J.: Stable isotope geochemistry, Springer International Publishing AG, part of Springer Nature, 8th ed., 2018.

Hofmann, H.: Stromatolites: characteristics and utility, Earth-Science Reviews, 9, 339–373, https://doi.org/10.1016/0012-8252(73)90002-0, 1973.

845 Hofmann, H., Grey, K., Hickman, A., and Thorpe, R.: Origin of 3.45 Ga coniform stromatolites in Warrawoona group, Western Australia, Geological Society of America Bulletin, 111, 1256–1262, https://doi.org/10.1130/0016-7606(1999)111<1256:OOGCSI>2.3.CO;2, 1999.

Kalkowsky, E.: Oolith und Stromatolith im norddeutschen Buntsandstein., Zeitschrift der deutschen geologischen Gesellschaft, pp. 68–125, 1908.

850 Kasting, J. F.: Early Earth Atmosphere and Oceans, in: Earth's Oldest Rocks, edited by Van Kranendonk, M.J., B. V. H. J., pp. 49–61, Elsevier, 2019.

Kasting, J. F., Eggler, D. H., and Raeburn, S. P.: Mantle Redox Evolution and the Oxidation State of the Archean Atmosphere, The Journal of Geology, 101, 245–257, https://doi.org/10.1086/648219, 1993.

Karato, S.: Physical properties of basalts from Deep Sea Drilling Project Hole 504B, Costa Rica Rift. *Init. Repts. DSDP* **69,**

855 687– 695, 1983.

Kato, Y. and Nakamura, K.: Origin and global tectonic significance of Early Archean cherts from the Marble Bar greenstone belt, Pilbara Craton, Western Australia, Precambrian Research, 125, 191–243, https://doi.org/10.1016/S0301-9268(03)00043-3, 2003.

Kempe, S.: Alkalinity: the link between anaerobic basins and shallow water carbonates?, Naturwissenschaften, 77, 426–427,

860 1990.

Kitajima, K., Maruyama, S., Utsunomiya, S., and Liou, J.: Seafloor hydrothermal alteration at an Archaean mid-ocean ridge, Journal of Metamorphic Geology, 19, 583–599, https://doi.org/10.1046/j.0263-4929.2001.00330.x, 2001.

Komiya, T., Maruyama, S., Hirata, T., and Yurimoto, H.: Petrology and geochemistry of MORB and OIB in the mid-Archean North Pole region, Pilbara craton, Western Australia: implications for the composition and temperature of the upper mantle at 3.5 Ga, International Geology Review, 44, 988–1016, https://doi.org/10.2747/0020-6814.44.11.988, 2002.

Korenaga, J.: Was there land on the early Earth?, Life, 11, 1142, https://doi.org/10.3390/life11111142, 2021.

Kozawa, T., Sugitani, K., Oehler, D. Z., House, C. H., Saito, I., Watanabe, T., and Gotoh, T.: Early Archean planktonic mode of life: Implications from fluid dynamics of lenticular microfossils, Geobiology, 17, 113–126, https://doi.org/10.1111/gbi.12319, 2019.

Kraml, M., Pik, R., Rahn, M., Selbekk, R., Carignan, J., and Keller, J.: A new multi-mineral age reference material for $^{40}$Ar/$^{39}$Ar, (U-Th)/He and fission track dating methods: the Limberg t3 tuff, Geostandards and Geoanalytical Research, 30, 73–86, https://doi.org/10.1111/j.1751- 908X.2006.tb00914.x, 2006.

Krissansen-Totton, J., Buick, R., and Catling, D.: A statistical analysis of the carbon isotope record from the Archean to Phanerozoic and implications for the rise of oxygen, American Journal of Science, 315, 275–316, https://doi.org/10.2475/04.2015.01, 2015.

Krissansen-Totton, J., Arney, G. N., and Catling, D. C.: Constraining the climate and ocean pH of the early Earth with a geological carbon cycle model, Proceedings of the National Academy of Sciences, 115, 4105–4110, https://doi.org/10.1073/pnas.1721296115, 2018.

Kroopnick, P.: The distribution of $^{13}$C in the Atlantic Ocean, Earth and Planetary Science Letters, 49, 469–484, https://doi.org/10.1016/0012- 821X(80)90088-6, 1980.

Kump, L., Barley, M. Increased subaerial volcanism and the rise of atmospheric oxygen 2.5 billion years ago. *Nature,* 448, 1033–1036, https://doi.org/10.1038/nature06058, 2007.

Lambert, I., Donnelly, T., Dunlop, J., Groves, and DI: Stable isotopic compositions of early Archaean sulphate deposits of probable evaporitic and volcanogenic origins, Nature, 276, 808–811, https://doi.org/10.1038/276808a0, 1978.

Ledevin, M.: Archean cherts: Formation processes and paleoenvironments, in: Earth's Oldest Rocks, edited by Van Kranendonk, M., Bennett, V., and Hoffmann, J., pp. 913–944, Elsevier, 2019.

Lees, A. and Buller, A. T.: Modern temperate-water and warm-water shelf carbonate sediments contrasted, Marine Geology, 13, M67–M73, https://doi.org/10.1016/0025-3227(72)90011-4, 1972.

Lepot, K., Williford, K. H., Ushikubo, T., Sugitani, K., Mimura, K., Spicuzza, M. J., and Valley, J. W.: Texture-specific isotopic compositions in 3.4 Gyr old organic matter support selective preservation in cell-like structures, Geochimica et Cosmochimica Acta, 112, 66–86, https://doi.org/10.1016/j.gca.2013.03.004, 2013.

Lepot, K.: Signatures of early microbial life from the Archean (4 to 2.5 Ga) eon, Earth-Science Reviews, 209, 103296, https://doi.org/10.1016/j.earscirev.2020.103296, 2020.

Lindsay, J., Brasier, M., McLoughlin, N., Green, O., Fogel, M., Steele, A., and Mertzman, S.: The problem of deep carbon—an Archean paradox, Precambrian Research, 143, 1–22, https://doi.org/10.1016/j.precamres.2005.09.003, 2005.

Lister, G. and Snoke, A.: SC mylonites, Journal of Structural Geology, 6, 617–638, https://doi.org/10.1016/0191-8141(84)90001-4, 1984.

Lowe, D. R.: Stromatolites 3,400-Myr old from the Archean of Western Australia, Nature, 284, 441–443, 1980.

Lowe, D. R.: Restricted shallow-water sedimentation of Early Archean stromatolitic and evaporitic strata of the Strelley Pool Chert, Pilbara Block, Western Australia, Precambrian Research, 19, 239–283, https://doi.org/10.1016/0301-9268(83)90016-5, 1983.

Lowe, D. R. and Tice, M. M.: Tectonic controls on atmospheric, climatic, and biological evolution 3.5–2.4Ga, Precambrian Research, 158, 177–197, https://doi.org/ 10.1016/j.precamres.2007.04.008, earliest Evidence of Life on Earth, 2007.

Lowe, D. R., Ibarra, D., Drabon, N., and Chamberlain, C.: Constraints on surface temperature 3.4 billion years ago based on triple oxygen isotopes of cherts from the Barberton Greenstone Belt, South Africa, and the problem of sample selection, American Journal of Science, 320, 790–814, https://doi.org/10.2475/11.2020.02, 2020.

Lunine, J. I. and Lunine, C. J.: The Archean Eon and the Origin of Life: I. Properties of and Sites for Life, in: Earth: Evolution of a Habitable World, pp. 134–152, Cambridge University Press, 1998.

Lünsdorf, N. K., Dunkl, I., Schmidt, B. C., Rantitsch, G., and von Eynatten, H.: Towards a higher comparability of geothermometric data obtained by Raman spectroscopy of carbonaceous material. Part 2: A revised geothermometer, Geostandards and Geoanalytical Research, 41, 593–612, https://doi.org/10.1111/ggr.12178, 2017.

Marien, C. S., Jäger, O., Tusch, J., Viehmann, S., Surma, J., Van Kranendonk, M. J., and Münker, C.: Interstitial carbonates in pillowed metabasaltic rocks from the Pilbara Craton, Western Australia: A vestige of Archean seawater chemistry and seawater-rock interactions, Precambrian Research, 394, 107 109, https://doi.org/10.1016/j.precamres.2023.107109, 2023.

Marshall, C. P., Love, G. D., Snape, C. E., Hill, A. C., Allwood, A. C., Walter, M. R., Van Kranendonk, M. J., Bowden, S. A., Sylva, S. P., and Summons, R. E.: Structural characterization of kerogen in 3.4 Ga Archaean cherts from the Pilbara Craton, Western Australia, Precambrian Research, 155, 1–23, https://doi.org/10.1016/j.precamres.2006.12.014, 2007.

McCollom, T. M. and Seewald, J. S.: Carbon isotope composition of organic compounds produced by abiotic synthesis under hydrothermal conditions, Earth and Planetary Science Letters, 243, 74–84, https://doi.org/10.1016/j.epsl.2006.01.027, 2006.

McCollom, T. M., Ritter, G., and Simoneit, B. R.: Lipid synthesis under hydrothermal conditions by Fischer-Tropsch-type reactions, Origins of Life and Evolution of the Biosphere, 29, 153–166, https://doi.org/10.1023/A:1006592502746, 1999.

McGrail, B. P., Schaef, H. T., Spane, F. A., Cliff, J. B., Qafoku, O., Horner, J. A., Thompson, C. J., Owen, A. T., and Sullivan, C. E.: Field validation of supercritical $CO_2$ reactivity with basalts, Environmental Science & Technology Letters, 4, 6–10, https://doi.org/10.1021/acs.estlett.6b00387, 2017.

McKeegan, K. D., Kudryavtsev, A. B., and Schopf, J. W.: Raman and ion microscopic imagery of graphitic inclusions in apatite from older than 3830 Ma Akilia supracrustal rocks, west Greenland, Geology, 35, 591–594, https://doi.org/10.1130/G23465A.1, 2007.

McNaughton, N., Compston, W., and Barley, M.: Constraints on the age of the Warrawoona Group, eastern Pilbara block, Western Australia, Precambrian Research, 60, 69–98, https://doi.org/10.1016/0301-9268(93)90045-4, 1993.

930 Menefee, A. H., Giammar, D. E., and Ellis, B. R.: Permanent $CO_2$ trapping through localized and chemical gradient-driven basalt carbona- tion, Environmental science & technology, 52, 8954–8964, https://doi.org/10.1021/acs.est.8b01814, 2018.

Mills, B., Lenton, T., and Watson, A.: Proterozoic oxygen rise linked to shifting balance between seafloor and terrestrial weathering, Proceedings of the National Academy of Sciences, 111, 9073—9078, https://doi.org/10.1073/pnas.1321679111, 2014.

935 Mißbach, H., Duda, J.-P., van den Kerkhof, A., Lüders, V., Pack, A., Reitner, J., and Thiel, V.: Ingredients for microbial life preserved in 3.5 billion-year-old fluid inclusions, Nature Communications, 12, https://api.semanticscholar.org/CorpusID:231947918, 2021.

Mojzsis, S. J., Arrhenius, G., McKeegan, K., Harrison, T., Nutman, A., and Friend, C.: Evidence for life on Earth before 3,800 million years ago, Nature, 384, 55–59, https://doi.org/10.1038/384055a0, 1996.

940 Moore, E. K., Jelen, B. I., Giovannelli, D., Raanan, H., and Falkowski, P. G.: Metal availability and the expanding network of microbial metabolisms in the Archaean eon, Nature Geoscience, 10, 629–636, https://doi.org/10.1038/ngeo3006, 2017.

Morag, N., Williford, K. H., Kitajima, K., Philippot, P., Van Kranendonk, M. J., Lepot, K., Thomazo, C., and Valley, J. W.: Microstructure- specific carbon isotopic signatures of organic matter from 3.5 Ga cherts of the Pilbara Craton support a biologic origin, Precambrian Research, 275, 429–449, https://doi.org/10.1016/j.precamres.2016.01.014, 2016.

945 Nakamura, K. and Kato, Y.: Carbonate minerals in the Warrawoona Group, Pilbara Craton: Implications for continental crust, life, and global carbon cycle in the Early Archean, Resource Geology, 52, 91–100, https://doi.org/10.1111/j.1751-3928.2002.tb00122.x, 2002.

Nakamura, K. and Kato, Y.: Carbonatization of oceanic crust by the seafloor hydrothermal activity and its significance as a $CO_2$ sink in the Early Archean, Geochimica et Cosmochimica Acta, 68, 4595–4618, https://doi.org/10.1016/j.gca.2004.05.023, 950 2004.

Neuweiler, F. and Reitner, J.: Initially indurated structures of fine-grained calcium carbonate formed in place (automicrite), Biomineralization 93: Abstract volume of the 7th International Symposium on Biomineralization: Musée Océanographique, Monaco, p. 159, 1993.

Neuweiler, F., Gautret, P., Thiel, V., Lange, R., Michaelis, W., and Reitner, J.: Petrology of Lower Cretaceous carbonate mud 955 mounds (Albian, N. Spain): insights into organomineralic deposits of the geological record, Sedimentology, 46, 837—859, https://doi.org/10.1046/j.1365- 3091.1999.00255.x, 1999.

Nijman, W. and de Vries, S. T.: Early Archaean crustal collapse structures and sedimentary basin dynamics, in: The Precambrian Earth: Tempos and Events, edited by Eriksson, P., Altermann, W., Nelson, D., Mueller, W., and Catuneau, O., pp. 139–154, Elsevier, Amsterdam, 2004.

960 Nisbet, E. and Sleep, N.: The habitat and nature of early life, Nature, 409, 1083–1091, https://doi.org/10.1038/35059210, 2001.

Nutman, A. P., Bennett, V. C., Friend, C. R., Van Kranendonk, M. J., and Chivas, A. R.: Rapid emergence of life shown by discovery of 3,700-million-year-old microbial structures, Nature, 537, 535–538, https://doi.org/10.1038/nature19355, 2016.

Nutman, A. P., Friend, C. R., Bennett, V. C., Van Kranendonk, M., and Chivas, A. R.: Reconstruction of a 3700 Ma transgressive marine environment from Isua (Greenland): Sedimentology, stratigraphy and geochemical signatures, Lithos,
965    346, 105164, https://doi.org/10.1016/j.lithos.2019.105164, 2019a.

Nutman, A. P., Bennett, V. C., Friend, C. R., Van Kranendonk, M. J., Rothacker, L., and Chivas, A. R.: Cross-examining Earth's oldest stromatolites: Seeing through the effects of heterogeneous deformation, metamorphism and metasomatism affecting    Isua    (Greenland)    3700    Ma    sedimentary    rocks,    Precambrian    Research,    331,    105   347, https://doi.org/10.1016/j.precamres.2019.105347, 2019b.

970    Nutman, A. P., Bennett, V. C., Friend, C. R., and Van Kranendonk, M. J.: In support of rare relict 3700 Ma stromatolites from Isua (Green- land), Earth and Planetary Science Letters, 562, 116 850, https://doi.org/10.1016/j.epsl.2021.116850, 2021.

Oehler, D. Z., Robert, F., Walter, M. R., Sugitani, K., Allwood, A., Meibom, A., Mostefaoui, S., Selo, M., Thomen, A., and Gibson, E. K.: NanoSIMS: insights to biogenicity and syngeneity of Archaean carbonaceous structures, Precambrian Research, 173, 70–78, https://doi.org/10.1016/j.precamres.2009.01.001, 2009.

975    Ohtomo, Y., Kakegawa, T., Ishida, A., Nagase, T., and Rosing, M. T.: Evidence for biogenic graphite in early Archaean Isua metasedimentary rocks, Nature Geoscience, 7, 25–28, https://doi.org/10.1038/ngeo2025, 2014.

Otálora, F., Mazurier, A., Garcia-Ruiz, J. M., Van Kranendonk, M., Kotopoulou, E., El Albani, A., and Garrido, C.: A crystallographic study of crystalline casts and pseudomorphs from the 3.5 Ga Dresser Formation, Pilbara Craton (Australia), Journal of Applied Crystallography, 51, 1050–1058, https://doi.org/10.1107/S1600576718007343, 2018.

980    Pratt, B. R.: Calcification of cyanobacterial filaments: *Girvanella* and the origin of lower Paleozoic lime mud, Geology, 29, 763—766, 2001.

Palme, H., and O'Neill, H.S.: Cosmochemical Estimates of Mantle Composition, Treatise on Geochemistry, 2, 1-39, http://dx.doi.org/10.1016/B978-0-08-095975-7.00201-1, 2014.

Pei, Y.: A geobiological approach to carbonate factories and ecosystem changes across the Permian–Triassic boundary, Ph.D.
985    thesis, University of Göttingen, Germany, http://dx.doi.org/10.53846/goediss-9160, 2022.

Pei, Y., Duda, J.-P., and Reitner, J.: Sedimentary factories and ecosystem change across the Permian–Triassic Critical Interval (P–TrCI): insights from the Xiakou area (South China), PalZ, pp. 709–725, https://doi.org/10.1007/s12542-020-00530-x, 2021.

Perry, R. S. and Sephton, M. A.: Reply to comments on defining biominerals and organominerals: Direct and indirect indicators of   life   [Perry   et   al.,   Sedimentary   Geology,   201,   157-179],   Sedimentary   Geology,   213,   156–156,
990    https://doi.org/10.1016/j.sedgeo.2008.11.005, 2009.

Perry, R. S., Mcloughlin, N., Lynne, B. Y., Sephton, M. A., Oliver, J. D., Perry, C. C., Campbell, K., Engel, M. H., Farmer, J. D., Brasier, M. D., and Staley, J.: Defining biominerals and organominerals: Direct and indirect indicators of life, Sedimentary Geology, 201, 157–179, https://doi.org/10.1016/j.sedgeo.2007.05.014, 2007.

Pinti, D. L., Hashizume, K., Sugihara, A., Massault, M., and Philippot, P.: Isotopic fractionation of nitrogen and carbon in Paleoarchean cherts from Pilbara craton, Western Australia: Origin of 15N-depleted nitrogen, Geochimica et Cosmochimica Acta, 73, 3819–3848, https://doi.org/10.1016/j.gca.2009.03.014, 2009.

Pomar, L. and Hallock, P.: Carbonate factories: a conundrum in sedimentary geology, Earth-Science Reviews, 87, 134–169, https://doi.org/10.1016/j.earscirev.2007.12.002, 2008.

Rasmussen, B., Fletcher, I. R., and Muhling, J. R.: In situ U–Pb dating and element mapping of three generations of monazite: unravelling cryptic tectonothermal events in low-grade terranes, Geochimica et Cosmochimica Acta, 71, 670–690, https://doi.org/10.1016/j.gca.2006.10.020, 2007.

Rausch, S.: Carbonate veins as recorders of seawater evolution, $CO_2$ uptake by the ocean crust, and seawater-crust interaction during low- temperature alteration, Ph.D. thesis, Universität Bremen, 2012.

Reijmer, J. J.: Marine carbonate factories: review and update, Sedimentology, 68, 1729–1796, https://doi.org/10.1111/sed.12878, 2021.

Reinhardt, M., Thiel, V., Duda, J.-P., Hofmann, A., Bajnai, D., Goetz, W., Pack, A., Reitner, J., Schanofski, M., Schönig, J., Whitehouse, M., and Drake, H.: Aspects of the biological carbon cycle in a ca. 3.42-billion-year-old marine ecosystem, Precambrian Research, 402, 107 289, https://doi.org/https://doi.org/10.1016/j.precamres.2024.107289, 2024.

Reitner, J.: Modern cryptic microbialite/metazoan facies from Lizard Island (Great Barrier Reef, Australia) formation and concepts, Facies, 29, 3-39, 1993.

Reitner, J.: Organomineralization: A clue to the understanding of meteorite-related "bacteria-shaped" carbonate particles, in: Origins: Genesis, Evolution and Diversity of Life, pp. 195–212, Springer, 2004.

Reitner, J. and Neuweiler, F.: Part I Mud mounds: recognizing a polygenetic spectrum of fine-grained carbonate buildups, in: Mudmounds: a polygenetic spectrum of fine-grained carbonate buildups, edited by Reitner, J. and Neuweiler, F., pp. 2–4, 1995.

Reitner, J. and Thiel, V.: Encyclopedia of Geobiology, Springer Amsterdam, 2011.

Reitner, J., Wilmsen, M., and Neuweiler, F.: Cenomanian/Turonian sponge microbialite deep-water hardground community (Liencres, Northern Spain), Facies, 32, 203–212, https://doi.org/10.1007/BF02536869, 1995a.

Reitner, J., Neuweiler, F., and Gautret, P.: Part II Modern and fossil automicrites: implications for mud mound genesis, in: Mud Mounds: A Polygenetic Spectrum of Fine-grained Carbonate Buildups, edited by Reitner, J. and Neuweiler, F., vol. 32, pp. 4–17, 1995b.

Reitner, J., Gautret, P., Marin, F., and Neuweiler, F.: Automicrites in a modern marine microbialite. Formation model via organic matrices (Lizard Island, Great Barrier Reef, Australia), Bulletin del'Institut océanographique, Monaco, n° spécial 14(2), 237–263, 1995c.

Reitner, J., Thiel, V., Zankl, H., Michaelis, W., Wörheide, G., and Gautret, P.: Organic and biogeochemical patterns in cryptic microbialites, in: Microbial sediments, edited by Riding, R. E. and Awramik, S. M., pp. 149–160, Springer, Berlin, https://doi.org/10.1007/978-3-662-04036-2_17, 2000.

Reitner, J., Wörheide, G., Lange, R., and Schumann-Kindel, G.: Coralline demosponges; a geobiological portrait, Bulletin/The Tohoku University Museum, pp. 219–235, https://doi.org/10.23689/fidgeo-2565, 2001.

Riding, R.: The term stromatolite: towards an essential definition, Lethaia, 32, 321–330, https://doi.org/10.1111/j.1502-3931.1999.tb00550.x, 1999.

Riding, R.: Microbial carbonates: the geological record of calcified bacterial–algal mats and biofilms, Sedimentology, 47, 179–214, https://doi.org/10.1046/j.1365-3091.2000.00003.x, 2000.

Rincón-Tomás, B., Khonsari, B., Mühlen, D., Wickbold, C., Schäfer, N., Hause-Reitner, D., Hoppert, M., and Reitner, J.: Manganese carbonates as possible biogenic relics in Archean settings, International Journal of Astrobiology, 15, 219–229, https://doi.org/10.1017/S1473550416000264, 2016.

Robbins, L. and Blackwelder, P.: Biochemical and ultrastructural evidence for the origin of whitings: A biologically induced calcium carbonate precipitation mechanism, Geology, 20, 464–468, https://doi.org/10.1130/0091-7613(1992)020<0464:BAUEFT>2.3.CO;2, 1992.

Roberts, R. G.: Ore deposit models11. Archean lode gold deposits, Geoscience Canada, 14, 37–52, https://id.erudit.org/iderudit/geocan14_1art02, 1987.

Rouillard, J., Van Kranendonk, M. J., Lalonde, S., Gong, J., and Van Zuilen, M. A.: Correlating trace element compositions, petrol- ogy, and Raman spectroscopy data in the 3.46 Ga Apex chert, Pilbara Craton, Australia, Precambrian Research, 366, 106415, https://doi.org/10.1016/j.precamres.2021.106415, 2021.

Runge, E. A., Duda, J.-P., Van Kranendonk, M. J., and Reitner, J.: Earth's oldest tsunami deposit? Early Archaean high-energy sediments in the ca 3.48 Ga Dresser Formation (Pilbara, Western Australia), The Depositional Record, 8, 590–602, https://doi.org/10.1002/dep2.175, 2022.

Runnegar, B., Dollase, W.A., Ketcham, R.A., Colbert, M., Carlson, W.D.: Early Archean sulfates from Western Australia first formed as hydrothermal barites not gypsum evaporites. In: Geological Society of America Abstracts with Programs, vol. 33, 2001.

Schidlowski, M.: A 3,800-million-year isotopic record of life from carbon in sedimentary rocks, Nature, 333, 313–318, https://api. semanticscholar.org/CorpusID:4233179, 1988.

Schlager, W.: Sedimentation rates and growth potential of tropical, cool-water and mud-mound carbonate systems, Geological Society, London, Special Publications, 178, 217–227, https://doi.org/10.1144/GSL.SP.2000.178.01.14, 2000.

Schlager, W.: Benthic carbonate factories of the Phanerozoic, International Journal of Earth Sciences, 92, 445–464, https://doi.org/10.1007/s00531-003-0327-x, 2003.

Schopf, J. W.: Microfossils of the Early Archean Apex chert: new evidence of the antiquity of life, Science, 260, 640–646, https://doi.org/10.1126/science.260.5108.640, 1993.

Schopf, J. W., Kudryavtsev, A. B., Agresti, D. G., Wdowiak, T. J., and Czaja, A. D.: Laser–Raman imagery of Earth's earliest fossils, Nature, 416, 73–76, https://doi.org/10.1038/416073a, 2002.

1060    Schopf, J. W., Kudryavtsev, A. B., Osterhout, J. T., Williford, K. H., Kitajima, K., Valley, J. W., and Sugitani, K.: An anaerobic 3400 Ma shallow-water microbial consortium: Presumptive evidence of Earth's Paleoarchean anoxic atmosphere, Precambrian Research, 299, 309–318, https://doi.org/10.1016/j.precamres.2017.07.021, 2017.

Schrag, D. P., Higgins, J. A., Macdonald, F. A., and Johnston, D. T.: Authigenic carbonate and the history of the global carbon cycle, Science, 339, 540–543, https://doi.org/10.1126/science.1229578, 2013.

1065    Sengupta, S., Peters, S. T., Reitner, J., Duda, J.-P., and Pack, A.: Triple oxygen isotopes of cherts through time, Chemical Geology, 554, 119 789, https://doi.org/https://doi.org/10.1016/j.chemgeo.2020.119789, 2020.

Shibuya, T., Tahata, M., Kitajima, K., Ueno, Y., Komiya, T., Yamamoto, S., Igisu, M., Terabayashi, M., Sawaki, Y., Takai, K., et al.: Depth variation of carbon and oxygen isotopes of calcites in Archean altered upper oceanic crust: Implications for the $CO_2$ flux from ocean to oceanic crust in the Archean, Earth and Planetary Science Letters, 321, 64–73,

1070    https://doi.org/10.1016/j.epsl.2011.12.034, 2012.

Shields, G. A.: Implications of Carbonate and Chert Isotope Records for the Early Earth, in: Earth's Oldest Rocks, edited by Van Kranendonk, M., Bennett, V., and Hoffmann, J., pp. 901–912, Elsevier, 2019.

Smithies, R., Champion, D., and Cassidy, K.: Formation of Earth's early Archaean continental crust, Precambrian Research, 127, 89–101, https://doi.org/10.1016/S0301-9268(03)00182-7, 2003.

1075    Smithies, R. H., Champion, D. C., Van Kranendonk, M. J., Howard, H. M., and Hickman, A. H.: Modern-style subduction processes in the Mesoarchean: geochemical evidence from the 3.12 Ga Whundo intra-oceanic arc, Earth and Planetary Science Letters, 231, 221–237, https://doi.org/10.1016/j.epsl.2004.12.026, 2005.

Smithies, R., Champion, D., Van Kranendonk, M., and Hickman, A.: Geochemistry of volcanic rocks of the northern Pilbara Craton, Western Australia, Geological Survey of Western Australia Report, 104, 1–47, 2007a.

1080    Smithies, R. H., Champion, D. C., and Van Kranendonk, M. J.: The oldest well-preserved felsic volcanic rocks on Earth: Geochemical clues to the early evolution of the Pilbara Supergroup and implications for the growth of a Paleoarchean protocontinent, in: Earth's Oldest Rocks, edited by Van Kranendonk, M., Smithies, R., and Bennett, V., vol. Developments in Precambrian Geology 15, pp. 339–367, Elsevier, Amsterdam, https://doi.org/10.1016/S0166-2635(07)15042-8, 2007b.

Stockmann, G. J., Wolff-Boenisch, D., Gislason, S. R., and Oelkers, E. H.: Do carbonate precipitates affect dissolution kinetics?

1085    1: Basaltic glass, Chemical Geology, 284, 306–316, https://doi.org/10.1016/j.chemgeo.2011.03.010, 2011.

Suarez, C. A., Edmonds, M., and Jones, A. P.: Earth Catastrophes and their Impact on the Carbon Cycle, Elements, 15, 301–306, https://doi.org/10.2138/gselements.15.5.301, 2019.

Sugitani, K., Lepot, K., Nagaoka, T., Mimura, K., Van Kranendonk, M., Oehler, D. Z., and Walter, M. R.: Biogenicity of morphologically diverse carbonaceous microstructures from the ca. 3400 Ma Strelley Pool Formation, in the Pilbara Craton,

1090    Western Australia, Astrobiology, 10, 899–920, https://doi.org/10.1089/ast.2010.0513, 2010.

Sugitani, K., Mimura, K., Nagaoka, T., Lepot, K., and Takeuchi, M.: Microfossil assemblage from the 3400 Ma Strelley Pool Formation in the Pilbara Craton, Western Australia: results form a new locality, Precambrian Research, 226, 59–74, https://doi.org/10.1016/j.precamres.2012.11.005, 2013.

Sugitani, K., Mimura, K., Takeuchi, M., Yamaguchi, T., Suzuki, K., Senda, R., Asahara, Y., Wallis, S., and Van Kranendonk, M.: A Paleoarchean coastal hydrothermal field inhabited by diverse microbial communities: the Strelley Pool Formation, Pilbara Craton, Western Australia, Geobiology, 13, 522–545, https://doi.org/10.1111/gbi.12150, 2015a.

Sugitani, K., Mimura, K., Takeuchi, M., Lepot, K., Ito, S., and Javaux, E.: Early evolution of large micro-organisms with cytological complexity revealed by microanalyses of 3.4 Ga organic-walled microfossils, Geobiology, 13, 507–521, https://doi.org/10.1111/gbi.12148, 2015b.

Sugitani, K., Kohama, T., Mimura, K., Takeuchi, M., Senda, R., and Morimoto, H.: Speciation of Paleoarchean life demonstrated by analysis of the morphological variation of lenticular microfossils from the Pilbara Craton, Australia, Astrobiology, 18, 1057–1070, https://doi.org/10.1089/ast.2017.1799, 2018.

Tan, F.C.: Stable carbon isotopes in dissolved inorganic carbon in marine and estuarine environments, In: Handbook of Enviromental Isotope Geochemistry, edited by Fritz, P., Fontes, J.C., vol. 3. pp. 171-190, 1988.

Taylor, S. R. and McLennan, S.: The composition and evolution of the continental crust: rare earth element evidence from sedimentary rocks, Philosophical Transactions of the Royal Society of London. Series A, Mathematical and Physical Sciences, 301, 381–399, https://doi.org/10.1098/rsta.1981.0119, 1981.

Terabayashi, M., Masada, Y., and Ozawa, H.: Archean ocean-floor metamorphism in the North Pole area, Pilbara Craton, western Australia, Precambrian Research, 127, 167–180, https://doi.org/10.1016/S0301-9268(03)00186-4, 2003.

Thompson, J. B., Schultze-Lam, S., Beveridge, T. J., and Des Marais, D. J.: Whiting events: biogenic origin due to the photosynthetic activity of cyanobacterial picoplankton, Limnology and oceanography, 42, 133–141, https://doi.org/10.4319/lo.1997.42.1.0133, 1997.

Thorpe, R., Hickman, A., Davis, D., Mortensen, J., and Trendall, A.: U-Pb zircon geochronology of Archaean felsic units in the Marble Bar region, Pilbara Craton, Western Australia, Precambrian Research, 56, 169–189, https://doi.org/10.1016/0301-9268(92)90100-3, 1992.

Tice, M. M., Thornton, D. C., Pope, M. C., Olszewski, T. D., and Gong, J.: Archean microbial mat communities, Annual review of earth and planetary sciences, 39, 297–319, https://doi.org/10.1146/annurev-earth-040809-152356, 2011.

Trichet, J. and Défarge, C.: Non-biologically supported organomineralization, Bulletin de l'Institut océanographique, Monaco. Numéro special 14(2), 203–236, 1995.

Ueno, Y., Isozaki, Y., Yurimoto, H., and Maruyama, S.: Carbon isotopic signatures of individual Archean microfossils (?) from Western Australia, International Geology Review, 43, 196–212, https://doi.org/10.1080/00206810109465008, 2001.

Ueno, Y., Yoshioka, H., Maruyama, S., and Isozaki, Y.: Carbon isotopes and petrography of kerogens in 3.5-Ga hydrothermal silica dikes in the North Pole area, Western Australia, Geochimica et Cosmochimica Acta, 68, 573–589, https://doi.org/10.1016/S0016-7037(03)00462- 9, 2004.

van den Boorn, S. H., van Bergen, M. J., Nijman, W., and Vroon, P. Z.: Dual role of seawater and hydrothermal fluids in Early Archean chert formation: evidence from silicon isotopes, Geology, 35, 939–942, https://doi.org/10.1130/G24096A.1, 2007.

Van Kranendonk, M. J.: Volcanic degassing, hydrothermal circulation and the flourishing of early life on Earth: A review of the evidence from c. 3490-3240 Ma rocks of the Pilbara Supergroup, Pilbara Craton, Western Australia, Earth-Science Reviews, 74, 197–240, https://doi.org/10.1016/j.earscirev.2005.09.005, 2006.

1130 Van Kranendonk, M. J.: A review of the evidence for putative Paleoarchean life in the Pilbara Craton, Western Australia, Developments in Precambrian Geology, 15, 855–877, https://doi.org/10.1016/S0166-2635(07)15072-6, 2007.

Van Kranendonk, M.: Stromatolite morphology as an indicator of biogenicity for Earth's oldest fossils from the 3.5-3.4 Ga Pilbara Craton, Western Australia, in: Advances in stromatolite geobiology. Lecture notes in earth sciences, edited by Reitner, J., Queric, N., and Arp, G., vol. 131, pp. 517–534, 2011.

1135 Van Kranendonk, M. J. and Pirajno, F.: Geochemistry of metabasalts and hydrothermal alteration zones associated with c. 3.45 Ga chert and barite deposits: implications for the geological setting of the Warrawoona Group, Pilbara Craton, Australia, Geochemistry: Exploration, Environment, Analysis, 4, 253–278, https://doi.org/10.1144/1467-7873/04-205, 2004.

Van Kranendonk, M. J., Hickman, A. H., Smithies, R. H., Nelson, D. R., and Pike, G.: Geology and tectonic evolution of the Archean North Pilbara terrain, Pilbara Craton, Western Australia, Economic Geology, 97, 695–732, 1140 https://doi.org/10.2113/gsecongeo.97.4.695, 2002.

Van Kranendonk, M. J., Webb, G. E., and Kamber, B. S.: Geological and trace element evidence for a marine sedimentary environment of deposition and biogenicity of 3.45 Ga stromatolitic carbonates in the Pilbara Craton, and support for a reducing Archaean ocean, Geobiology, 1, 91–108, https://doi.org/10.1046/j.1472-4669.2003.00014.x, 2003.

Van Kranendonk, M. J., Hickman, A. H., and Huston, D. L.: Geology and Mineralization of the East Pilbara d A Field Guide, 1145 Western Australia Geological Survey. Record 2006/16, 94p, 2006.

Van Kranendonk, M. J., Hugh Smithies, R., Hickman, A. H., and Champion, D.: Secular tectonic evolution of Archean continental crust: interplay between horizontal and vertical processes in the formation of the Pilbara Craton, Australia, Terra Nova, 19, 1–38, https://doi.org/10.1111/j.1365-3121.2006.00723.x, 2007a.

Van Kranendonk, M. J., Smithies, R. H., Hickman, A. H., and Champion, D. C.: Paleoarchean development of a continental 1150 nucleus: the East Pilbara terrane of the Pilbara craton, Western Australia, Developments in Precambrian geology, 15, 307–337, https://doi.org/10.1016/S0166-2635(07)15041-6, 2007b.

Van Kranendonk, M. J., Philippot, P., Lepot, K., Bodorkos, S., and Pirajno, F.: Geological setting of Earth's oldest fossils in the ca. 3.5 Ga Dresser formation, Pilbara Craton, Western Australia, Precambrian Research, 167, 93–124, https://doi.org/10.1016/j.precamres.2008.07.003, 2008.

1155 Van Kranendonk, M. J., Smithies, R. H., Hickman, A. H., and Champion, D. C.: Paleoarchean development of a continental nucleus: the East Pilbara Terrane of the Pilbara Craton, Western Australia, in: Earth's Oldest Rocks, edited by Van Kranendonk, M.J., Bennett, V.C., Hoffmann, J.E., pp. 437–462, Elsevier, 2019a.

Van Kranendonk, M., Djokic, T., Poole, G., Tadbiri, S., Steller, L., and Baumgartner, R.: Depositional Setting of the Fossiliferous, c.3480 Ma Dresser Formation, Pilbara Craton: A Review, in: Earth's Oldest Rocks, edited by Van Kranendonk, 1160 M.J., Bennett, V.C., Hoffmann, J.E., pp. 985–1006, Elsevier, 2019b.

van Zuilen, M. A.: Proposed early signs of life not set in stone, Nature, pp. 190–191, https://doi.org/10.1038/d41586-018-06994-x, 2018.

van Zuilen, M.: The Significance of Carbonaceous Matter to Understanding Life Processes on Early Earth. In: Van Kranendonk, M.J., Bennett, V.C., Hoffmann, J.E. (Eds.), in: Earth's Oldest Rocks. Elsevier, 945–963, 2019.

1165    Veizer, J., Compston, W., Hoefs, J., and Nielsen, H.: Mantle buffering of the early oceans, Naturwissenschaften, 69, 173–180, https://doi.org/10.1007/BF00364890, 1982.

Veizer, J., Hoefs, J., Ridler, R., Jensen, L., and Lowe, D.: Geochemistry of Precambrian carbonates: I. Archean hydrothermal systems, Geochimica et Cosmochimica Acta, 53, 845–857, https://doi.org/10.1016/0016-7037(89)90030-6, 1989a.

Veizer, J., Hoefs, J., Lowe, D., and Thurston, P.: Geochemistry of Precambrian carbonates: II. Archean greenstone belts and
1170    Archean sea water, Geochimica et Cosmochimica Acta, 53, 859–871, https://doi.org/10.1016/0016-7037(89)90031-8, 1989b.

Viehmann, S., Reitner, J., Tepe, N., Hohl, S. V., Van Kranendonk, M., Hofmann, T., Koeberl, C., and Meister, P.: Carbonates and cherts as archives of seawater chemistry and habitability on a carbonate platform 3.35 Ga ago: Insights from Sm/Nd dating and trace element analysis from the Strelley Pool Formation, Western Australia, Precambrian Research, 344, 105742, https://doi.org/10.1016/j.precamres.2020.105742, 2020.

1175    Voigt, M., Pearce, C. R., Baldermann, A., and Oelkers, E. H.: Stable and radiogenic strontium isotope fractionation during hydrothermal seawater-basalt interaction, Geochimica et Cosmochimica Acta, 240, 131–151, https://doi.org/10.1016/j.gca.2018.08.018, 2018.

Wacey, D.: Stromatolites in the 3400 Ma Strelley Pool Formation, Western Australia: examining biogenicity from the macro-to the nano- scale, Astrobiology, 10, 381–395, https://doi.org/10.1089/ast.2009.0423, 2010.

1180    Wacey, D., McLoughlin, N., Whitehouse, M. J., and Kilburn, M. R.: Two coexisting sulfur metabolisms in a ca. 3400 Ma sandstone, Geology, 38, 1115–1118, https://doi.org/10.1130/G31329.1, 2010.

Wacey, D., Kilburn, M. R., Saunders, M., Cliff, J., and Brasier, M. D.: Microfossils of sulphur-metabolizing cells in 3.4-billion-year-old rocks of Western Australia, Nature Geoscience, 4, 698–702, https://doi.org/10.1038/ngeo1238, 2011.

Wacey, D., Noffke, N., Saunders, M., Guagliardo, P., and Pyle, D. M.: Volcanogenic pseudo-fossils from the 3.48 Ga dresser
1185    formation, Pilbara, Western Australia, Astrobiology, 18, 539–555, https://doi.org/10.1089/ast.2017.1734, 2018.

Wang, J., Tarhan, L. G., Jacobson, A. D., Oehlert, A. M., and Planavsky, N. J.: The evolution of the marine carbonate factory, Nature, pp. 1–5, https://doi.org/10.1038/s41586-022-05654-5, 2023.

Weimann, L., Reinhardt, M., Duda, J.-P., Mißbach-Karmrodt, H., Drake, H., Schönig, J., Holburg, J., Andreas, L., Reitner, J., Whitehouse, M., and Thiel, V.: Carbonaceous matter in ∼ 3.5 Ga black bedded barite from the Dresser Formation (Pil- bara
1190    Craton, Western Australia) – Insights into organic cycling on the juvenile Earth, Precambrian Research, 403, 107321, https://doi.org/https://doi.org/10.1016/j.precamres.2024.107321, 2024.

Weiner, S. and Dove, P. M.: An overview of biomineralization processes and the problem of the vital effect, Reviews in mineralogy and geochemistry, 54, 1–29, https://doi.org/10.2113/0540001, 2003.

Wojdyr, M.: Fityk: a general-purpose peak fitting program, Journal of Applied Crystallography, 43, 1126–1128,

1195    https://doi.org/10.1107/S0021889810030499, 2010.

Wolff-Boenisch, D. and Galeczka, I.: Flow-through reactor experiments on basalt-(sea)water-$CO_2$ reactions at 90 °C and neutral pH. What happens to the basalt pore space under post-injection conditions?, International Journal of Greenhouse Gas Control, 68, 176–190, https://doi.org/10.1016/j.ijggc.2017.11.013, 2018.

Xiang, W.: Carbonate factories in the early Archean and their geobiological impacts, Ph.D. thesis, University of Göttingen,

1200    Germany, http://dx.doi.org/10.53846/goediss-10047, 2023.

Xiong, W., Wells, R. K., Horner, J. A., Schaef, H. T., Skemer, P. A., and Giammar, D. E.: $CO_2$ mineral sequestration in naturally porous basalt, Environmental Science & Technology Letters, 5, 142–147, https://doi.org/10.1021/acs.estlett.8b00047, 2018.

Yamamoto, K., Itoh, N., Matsumoto, T., Tanaka, T., and Adachi, M.: Geochemistry of Precambrian carbonate intercalated in

1205    pillows and its host basalt: implications for the REE composition of circa 3.4 Ga seawater, Precambrian Research, 135, 331–344, https://doi.org/10.1016/j.precamres.2004.09.006, 2004.

Zahnle, K. J., Catling, D. C., and Claire, M. W.: The rise of oxygen and the hydrogen hourglass, Chemical Geology, 362, 26–34, https: //api.semanticscholar.org/CorpusID:55825754, 2013.

Zawaski, M. J., Kelly, N. M., Orlandini, O. F., Nichols, C. I., Allwood, A. C., and Mojzsis, S. J.: Reappraisal of purported ca.

1210    3.7 Ga stromatolites from the Isua Supracrustal Belt (West Greenland) from detailed chemical and structural analysis, Earth and Planetary Science Letters, 545, 116 409, https://doi.org/10.1016/j.epsl.2020.116409, 2020.

Zawaski, M. J., Kelly, N. M., Orlandini, O. F., Nichols, C. I., Allwood, A. C., and Mojzsis, S. J.: Reply: The Isua (Greenland)" relict stromatolites" cannot be confidently interpreted as original sedimentary structures, Earth and Planetary Science Letters, 562, 116 851, https://doi.org/10.1016/j.epsl.2021.116851, 2021.